

Associate Scientist mission report

Document NWPSAF-KN-VS-009

Version 1.0

6 July 2012

# Polarization options for the EPS-SG scatterometer

Maria Belmonte Rivas, Ad Stoffelen and Gerd-Jan Van Zadelhoff



The EUMETSAT Network of Satellite Application Facilities	 <b>NWP SAF</b> Numerical Weather Prediction	<b>Polarization options for the EPS-SG scatterometer</b>	Doc ID :NWPSAF-KN-VS-009 Version : 1.0 Date : 6 July 2012
---	--	--	---

This documentation was developed within the context of the EUMETSAT Satellite Application Facility on Numerical Weather Prediction (NWP SAF), under the Cooperation Agreement dated 29 June 2011, between EUMETSAT and the Met Office, UK, by one or more partners within the NWP SAF. The partners in the NWP SAF are the Met Office, ECMWF, KNMI and Météo France.

Copyright 2012, EUMETSAT, All Rights Reserved.

Change record			
Version	Date	Author / changed by	Remarks
1.0	6.7.12	M.Belmonte Rivas, A.Stoffelen and G-J.Van Zadelhoff	



# Final Report

## Polarization options for the EPS-SG scatterometer

Authors: Maria Belmonte Rivas, Ad Stoffelen, Gerd-Jan Van Zadelhoff

*Abstract* – This report provides an end-to-end performance evaluation for the introduction of HH and VH polarization capabilities on an ASCAT-type scatterometer, focusing on wind retrieval at high wind speeds (25 to 65 m/s). The Geophysical Model Functions (GMFs) for C-band VV, HH and VH polarized backscatter used in scatterometer wind retrieval simulations are defined, and a final recommendation regarding an optimal antenna configuration is made.

### Table of Contents

- 1 – Introduction
- 2 – Definition of Geophysical Model Functions
  - 2.1 - VV polarization GMF
  - 2.2 - HH polarization GMF
  - 2.3 - VH polarization GMF
- 3 – Simulation and wind retrieval performance
  - 3.1 – Proposed antenna configurations
  - 3.2 – Simulation results
    - Wind Vector RMS (VRMS)
    - Wind Speed RMS (WSRMS)
  - 3.3 – Discussion
- 4 - Conclusions
  
- References
- Appendices



## 1 - Introduction

The EPS-SG scatterometer wind retrieval is anticipated to be one of the main NWP SAF products in the 2020-2040 time frame. Simulations of wind retrieval performance are being used to consolidate the baseline EPS-SG scatterometer concept (Phase A) and support decisions on the optional system requirements specified in the Systems Requirement Document (SRD), in particular an extended capability at extreme high winds.

The baseline instrument design selected at the end of Phase 0 is a C-band (5.3 GHz) fixed fan-beam scatterometer with six antennas, similar to ASCAT on MetOp [Lin, 2011]. The baseline scatterometer concept covers an incidence angle range of 20-65 degrees at the surface and a specified dynamic wind speed range of 4-25 m/s. The baseline polarization is VV, i.e. vertical polarizations in transmit and receive. In addition, the implementation of VH and HH polarization options is considered here for extending the upper dynamic range of wind measurements to 25-65 m/s.

This report describes the derivation of C-band VV, HH and VH Geophysical Model Functions (GMFs) based on a literature survey of existing airborne and spaceborne empirical data [Liu, 2000]. The empirical GMFs described in this report are used in the synthesis of backscatter measurements, which serve as input to an end-to-end wind retrieval simulator that facilitates an objective assessment of the merits ascribed to different antenna configurations.

## 2 – Definition of Geophysical Model Functions

### 2.1 - VV polarization GMF

The GMF for vertically polarized ocean backscatter, denoted CMOD5.N ([Hersbach, 2007], [Portabella, 2009])<sup>1</sup>, was determined on the basis of a comparison between ERS-2 AMI backscatter and collocated buoy and ECMWF first-guess winds. For winds larger than 25 m/s, the experimental findings of [Donnelly, 1999] were used as a guideline. The collocated data was stratified according to incidence angle  $\theta$  and equivalent neutral wind speed  $U_{10N}$ , and the dependence on wind direction  $\phi$  modeled as:

---

<sup>1</sup> CMOD5.N input winds are 0.7 m/s higher than CMOD5 inputs for the same backscatter, but identical in all other respects.

$$\sigma_{VV}^0(\theta, U_{10N}, \phi) = B_0(\theta, U_{10N}) [1 + B_1(\theta, U_{10N}) \cos \phi + B_2(\theta, U_{10N}) \cos 2\phi]^p \quad (1)$$

Where  $\phi$  is the wind direction relative to the antenna beam. The  $B_0$  term describes the isotropic backscatter response for a given wind speed, while the  $B_1$  and  $B_2$  terms describe the amplitude of the upwind-downwind and upwind-crosswind modulations respectively<sup>2</sup>. The complete functional form of CMOD5.N is given in Appendix A. The CMOD5.N GMF is used operationally for the retrieval of ocean surface vector winds between 0 and 60 m/s observed at incidence angles between 20 and 65 degrees.

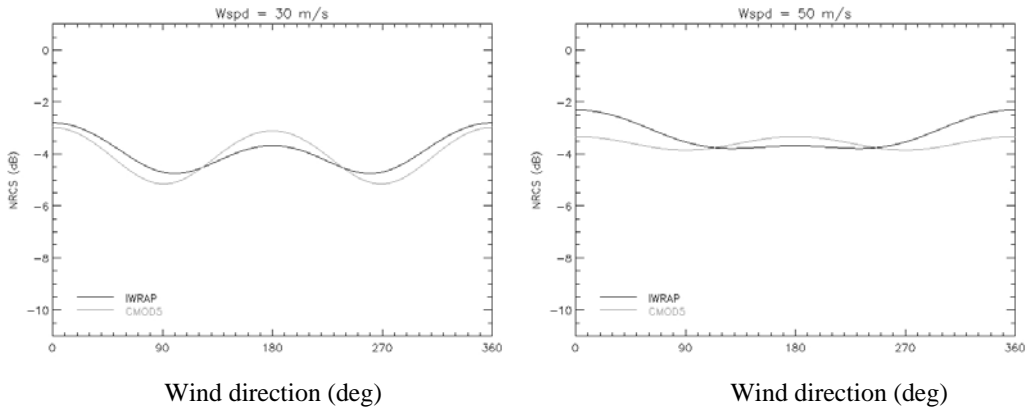


**Fig.1** – CMOD5.N and IWRAP C-band VV backscatter at 29 deg incidence (left 30 m/s, right 50 m/s)

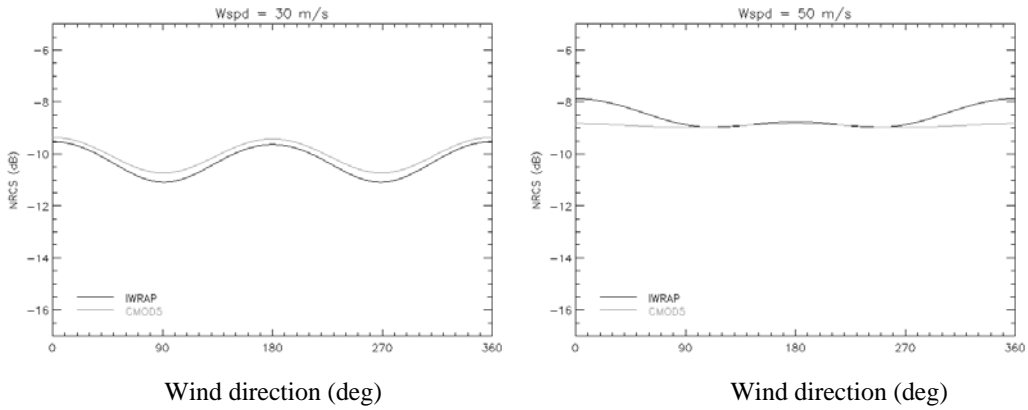


**Fig.2** – CMOD5.N and IWRAP C-band VV backscatter at 50 deg incidence (left 30 m/s, right 50 m/s)

The CMOD5.N normalized radar cross section (NRCS) at high wind speeds is plotted in Figs. 1-2 as a function of wind direction. For comparison, the ocean normalized radar cross section derived from the IWRAP dataset [Esteban, 2006] is also shown. The IWRAP VV high wind speed model is based on airborne ocean backscatter measurements taken at incidence angles between 29 and

<sup>2</sup> The conventional way to expand the ocean backscatter function is:  $\sigma^0 = A_0 + A_1 \cos \phi + A_2 \cos 2\phi$   
With terms that relate to Eq.(1) as [Stoffelen, 1998]:  $A_0 = B_0$  ;  $A_1 / A_0 \approx B_1 \cdot p$  ;  $A_2 / A_0 \approx B_2 \cdot p$

50 deg, and high to very high wind speed conditions (25 to 65 m/s) during missions through several tropical cyclones. Its complete functional form is given in Appendix B.

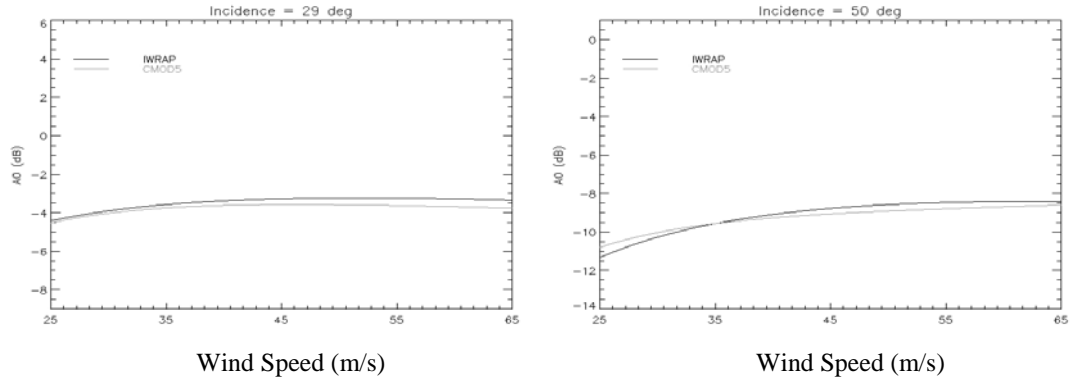


**Fig.3** – CMOD5.N and IWRAP isotropic  $B_0$  term (VV) as a function of wind speed at 29 and 50 deg incidence.

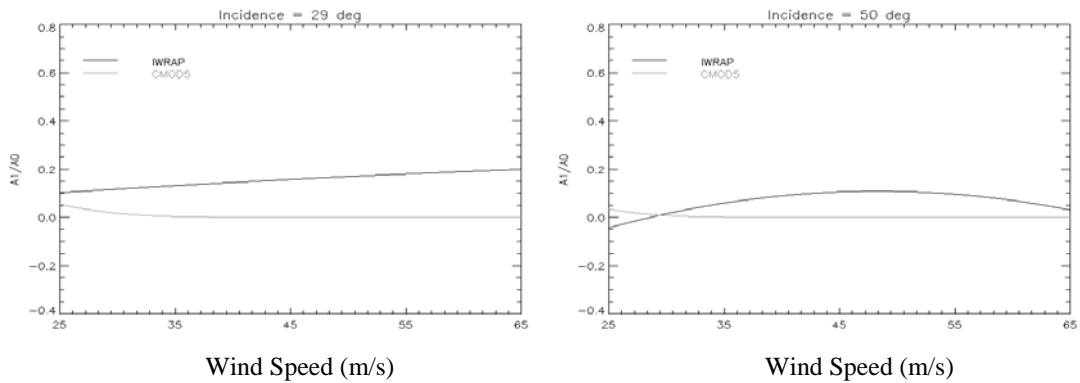


**Fig.4** – CMOD5.N and IWRAP up/downwind  $B_1$  term (VV) as a function of wind speed at 29 and 50 deg incidence.

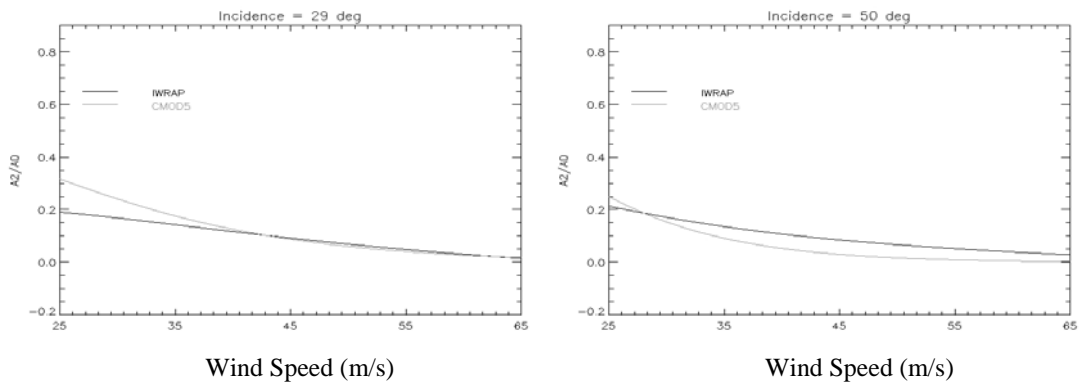


**Fig.5** – CMOD5 and IWRAP up/crosswind  $B_2$  term (VV) as a function of wind speed at 29 and 50 deg incidence.

The maximum disagreement between the CMOD5.N and IWRAP backscatter models is about 1 dB, with largest discrepancies seen for upwind backscatter at extreme high wind speeds. The ocean NRCS contributions to the isotropic  $B_0$ , up/downwind  $B_1$  and up/crosswind  $B_2$  terms are displayed separately in Figs. 3-5 as a function of wind speed. The amplitude of the up/downwind modulation reported by IWRAP is larger than predicted by CMOD5.N at high wind speeds (see Fig.4), contributing to the largest discrepancies between CMOD5.N and IWRAP. This feature is considered of little importance to wind retrieval sensitivity. The general agreement between the CMOD5.N and IWRAP models at VV is considered satisfactory up to wind speeds of 65 m/s.

Both the CMOD5.N and IWRAP models show that isotropic backscatter at VV polarization saturates at extreme high winds (see Fig.3), and over-saturates at the lowest incidence angles ( $\theta < 40$  deg). Owing to saturation, the ocean backscatter at VV polarization becomes insensitive to extreme wind direction as both the  $B_1$  and  $B_2$  terms approach zero. The CMOD5.N up/crosswind  $B_2$  modulation has a maximum between 10 and 15 m/s (not shown) and approaches zero for large wind speeds, although more rapidly in CMOD5.N than reported by IWRAP. IWRAP measurements also indicate that the up/downwind  $B_1$  modulation does not vanish at high wind speeds, even though the isotropic response saturates.

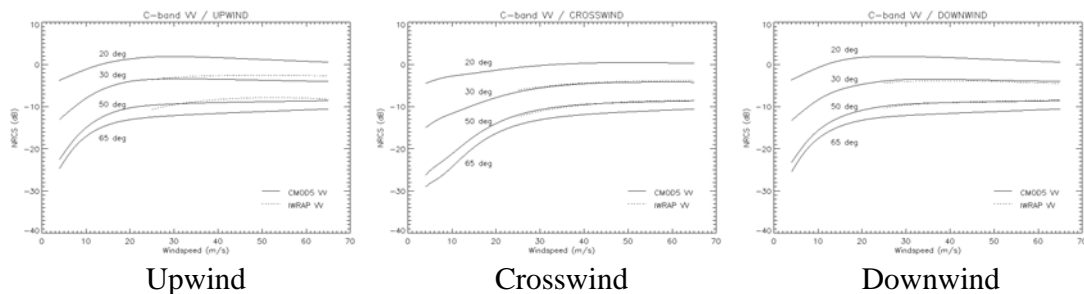


**Fig. 6** - CMOD5.N and IWRAP C-band VV backscatter as a function of wind speed

In summary, the CMOD5.N GMF at VV polarization is the only available model that provides ocean backscatter estimates for the entire incidence angle range of the EPS-SG scatterometer (from 20 to 65 degrees). The IWRAP ocean backscatter data provides a good fit (maximum departures  $< 1$  dB, mainly relating to differences in upwind ocean backscatter) to CMOD5.N for winds between 25 and 65 m/s and incidence angles between 29 and 50 deg. The CMOD5.N up/downwind component is slightly smaller than reported by IWRAP, but this term is considered not critical for wind retrieval sensitivity.

## 2.2 - HH polarization GMF

The GMF for horizontally polarized ocean backscatter (that is, horizontal polarizations in transmit and receive, denoted HH) is obtained through incorporation of an empirical model of the ocean co-polarization ratio (CPR), defined as:

$$CPR = \sigma_{VV}^0(\theta, U_{10}, \phi) / \sigma_{HH}^0(\theta, U_{10}, \phi) \quad (2)$$

The co-polarization ratio is used to scale the backscatter response from VV to HH as:

$$\sigma_{HH}^0(\theta, U_{10}, \phi) = (1/CPR) \cdot \sigma_{VV}^0(\theta, U_{10}, \phi) \quad (3)$$

Where  $\sigma_{VV}^0$  is the VV polarization GMF, namely the CMOD5.N model as defined in the previous section. Based on airborne C-band ocean backscatter simultaneously collected at HH and VV (STORM campaign, [Mouche, 2005]) the ocean CPR at C-band was found to be weakly dependent on wind speed, yet a function of incidence and wind direction and expressed as:

$$CPR(\theta, \phi) = C_0(\theta) + C_1(\theta) \cos \phi + C_2(\theta) \cos 2\phi \quad (4)$$

Where

$$\begin{aligned} C_0(\theta) &= [P(0) + P(180) + 2P(90)] / 4 \\ C_1(\theta) &= [P(0) - P(180)] / 2 \\ C_2(\theta) &= [P(0) + P(180) - 2P(90)] / 4 \end{aligned} \quad (5)$$

And

$$P(\phi) = A(\phi) \cdot \exp[B(\phi) \cdot \theta] + C(\phi) \quad (6)$$

The coefficients for the C-band ocean co-polarization model are given in Table 1.

**Table 1** – Coefficients A( $\phi$ ), B( $\phi$ ), C( $\phi$ ) for the CPR model of [Mouche, 2005]

	A( $\phi$ )	B( $\phi$ )	C( $\phi$ )
$\phi=0$	6.50704E-3	1.28983E-1	9.92839E-1
$\phi=90$	7.82194E-3	1.21405E-1	9.92839E-1
$\phi=180$	5.98416E-3	1.40952E-1	9.92885E-1

This model for the co-polarization ratio of the ocean backscatter at C-band, denoted  $CPR_{\text{Mouche}}$  and plotted in Fig.7, is considered valid for incidence angles from 10 to 43 degrees and low to moderate winds (4 to 16 m/s).

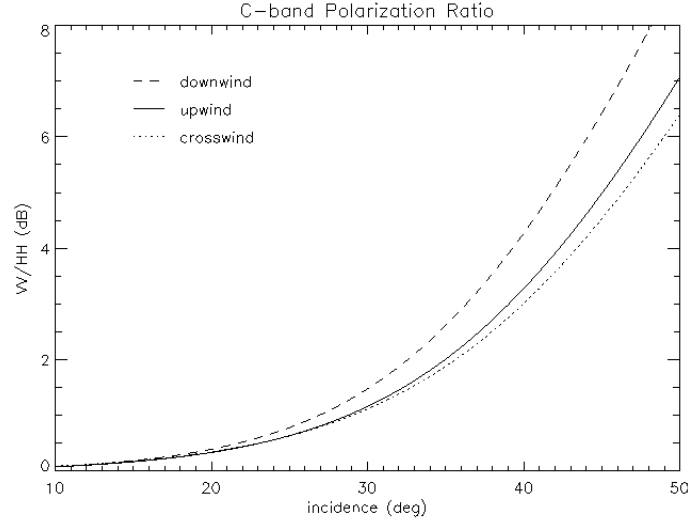


**Fig. 7** – C-band ocean co-polarization ratio (CPR) after [Mouche, 2005]

The CPR model proposed by [Mouche, 2005] assumes that the ocean co-polarization ratio does not depend on wind speed. A wind speed correction was proposed by [Hwang, 2010] based on RADARSAT-2 data (valid for incidences between 20 and 40 degrees and winds from 0 to 20 m/s). The wind speed correction substitutes the  $C_0$  term in Eq.(5) with:

$$\tilde{C}_0(\theta, U_{10}) = f_1(\theta) \cdot U_{10}^{f_2(\theta)} \quad (7)$$

Where

$$\begin{aligned} f_1(\theta) &= 1.56 \times 10^{-3} \theta^2 - 3.39 \times 10^{-2} \theta + 1.33 \\ f_2(\theta) &= -1.15 \times 10^{-3} \theta - 7.24 \times 10^{-2} \end{aligned} \quad (8)$$

The C-band ocean CPR of [Mouche, 2005] modified by the wind speed correction term proposed by [Hwang, 2010] is plotted in Fig.8 for later reference.

Note that none of the CPR models proposed this far is valid for winds stronger than 20 m/s, or incidence angles larger than 40 degrees. In the domain of high wind speeds ( $U_{10} > 25$  m/s), the IWRAP VV and HH models provide a useful reference and their functional form is given in Appendix B. Recall that the IWRAP VV and HH high wind speed models are based on airborne

ocean backscatter measurements taken at incidence angles from 29 to 50 deg [Esteban, 2006]. The ocean CPR model proposed by [Esteban, 2006] and based on IWRAP is plotted in Fig.9 against the ocean CPR model proposed by [Mouche, 2005]. Large differences become apparent between these models in their common domain of validity, between 30 and 40 deg of incidence. Most strikingly, the IWRAP-based ocean CPR does not approach unity at low incidence angles, as predicted by all the Bragg-based theoretical models and actually confirmed by the [Mouche, 2005] empirical dataset. Since an increase in wind speed should lead to lower CPR values (as shown in Fig.8 and Fig.9), we should reject the IWRAP results in the domain of low incidence angles (from 20 to 40 degrees) and take the Mouche model as an upper bound to high wind speed CPRs. The lack of empirical data (C-band HH and VV backscatter from the ocean) in the domain of large incidence angles and low wind speeds also demands that we take the IWRAP model results as indicative of low wind speed CPRs in the domain of high incidence angles.

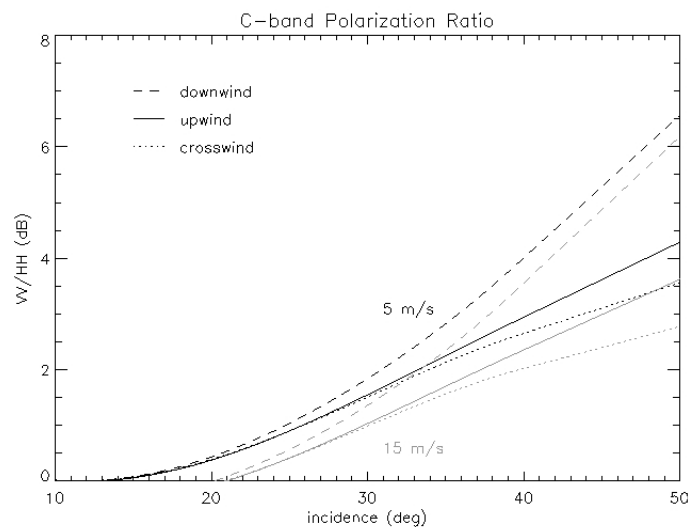


**Fig. 8** – C-band ocean co-polarization ratio (CPR) with wind speed correction after [Hwang, 2010]

To complete the formulation of the extended C-band ocean CPR model, the IWRAP CPR data must be linearly extrapolated into the range of 50 to 65 degrees of incidence. The resulting C-band ocean CPR model bears IWRAP's polarization signature at high winds and high incidences, and approaches Mouche's wind independent polarization ratio at low winds and low incidences, as shown in Fig. 10.

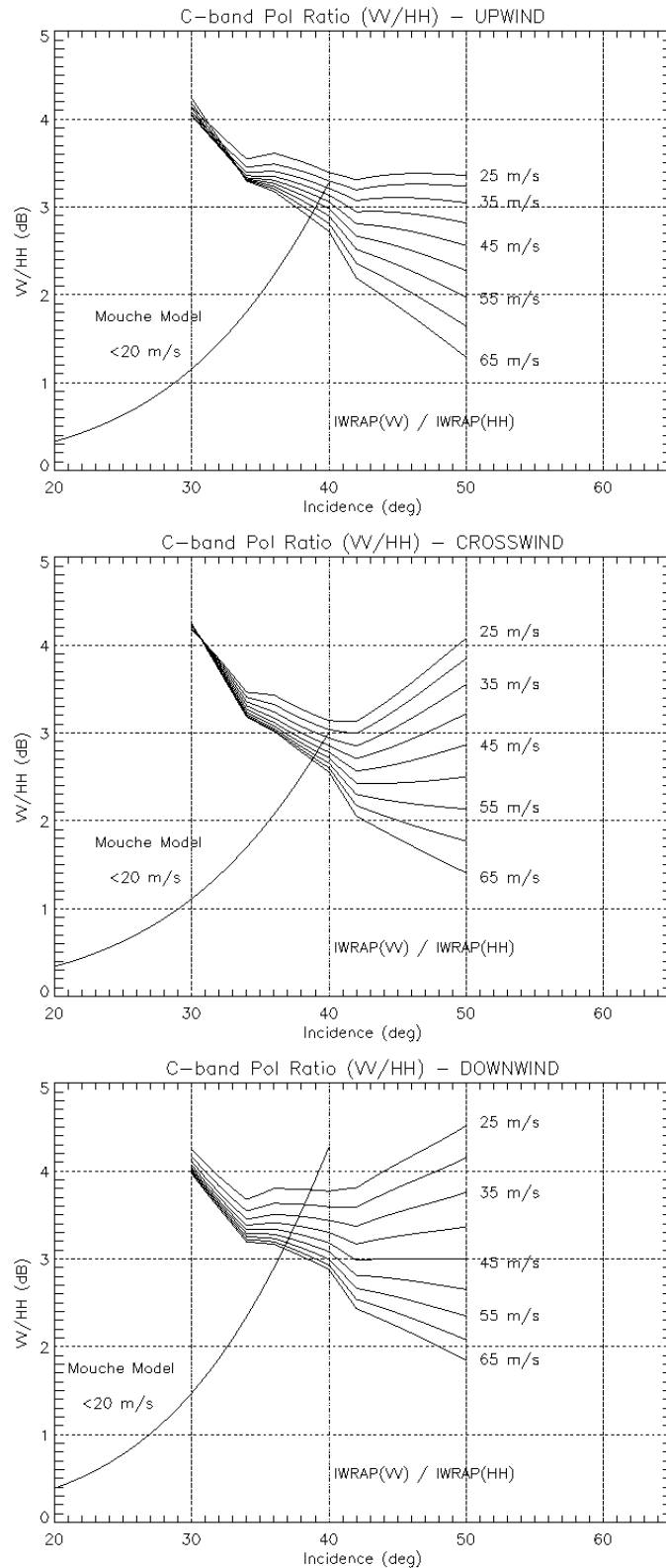


**Fig. 9** - The ocean CPR model based on STORM data and proposed by [Mouche, 2005] against the ocean CPR model based on IWRAP data and proposed by [Esteban, 2006].

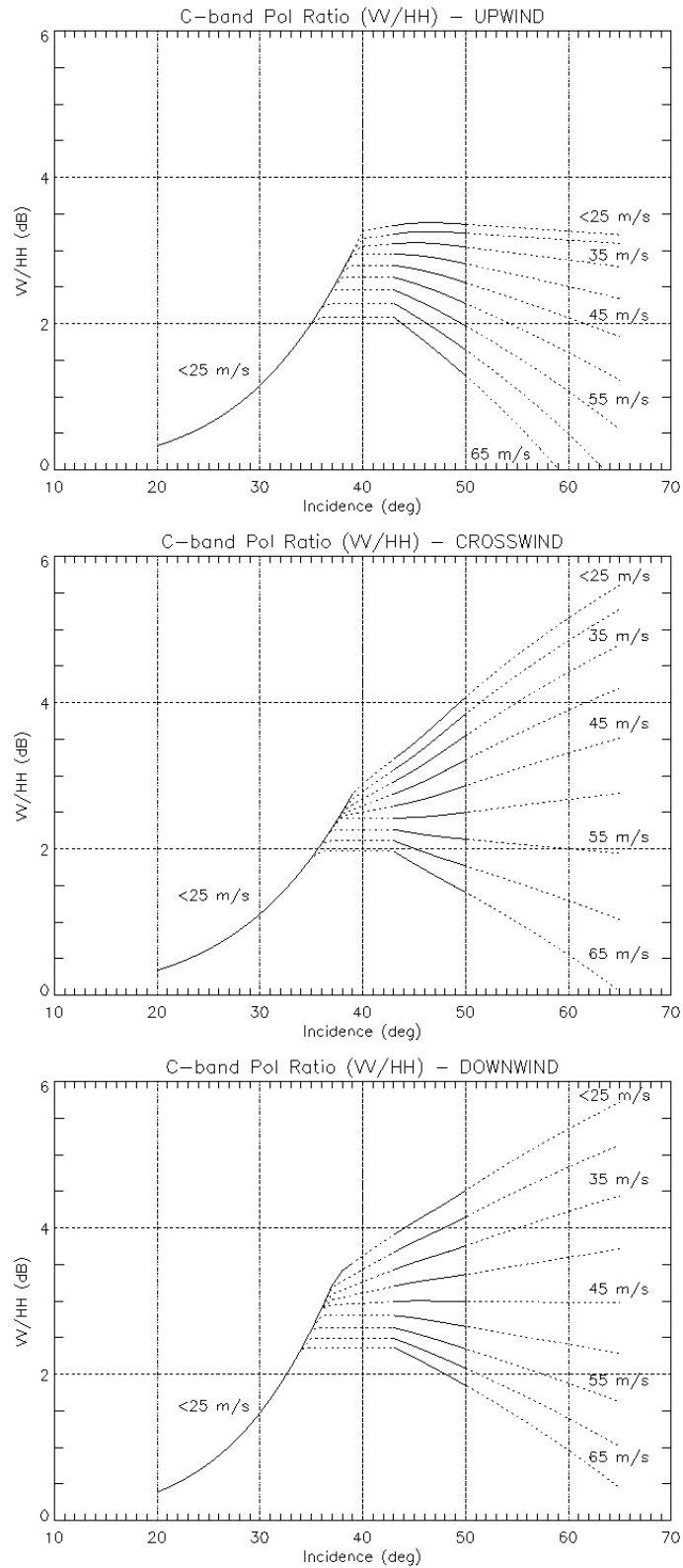


**Fig. 10** - The extended C-band ocean CPR model based on STORM (low incidence angles 20-40°, and low winds  $U_{10} < 20$  m/s) and IWRAP data (high incidence angles 42-50°, and high winds  $U_{10} > 25$  m/s)

In summary, we define an extended ocean CPR model for wind speeds between 4 and 65 m/s such that:

$$\begin{aligned} CPR(\theta, U_{10}, \phi) \Big|_{20 < \theta < 40^\circ} &= CPR_{Mouche}(\theta, \phi) \\ CPR(\theta, U_{10}, \phi) \Big|_{42 < \theta < 50^\circ} &= CPR_{IWRAP}(\theta, U_{10}, \phi) \end{aligned} \quad (9)$$

The ocean co-polarization ratio in the 50 to 65 deg range of incidence angles is based on linear extrapolation of IWRAP data as:

$$CPR(\theta, U_{10}, \phi) \Big|_{\theta > 50^\circ} = CPR_{IWRAP}(50^\circ, U_{10}, \phi) + (\theta - 50) \cdot \left. \frac{\partial CPR_{IWRAP}(\theta, U_{10}, \phi)}{\partial \theta} \right|_{\theta=50^\circ} \quad (10)$$

And the transition between the low and high incidence angle regimes is effected by linearly extrapolating the IWRAP CPR model towards lower incidence angles as:

$$CPR(\theta, U_{10}, \phi) \Big|_{\theta_c < \theta < 42^\circ} = CPR_{IWRAP}(42^\circ, U_{10}, \phi) + (\theta - 42) \cdot \left. \frac{\partial CPR_{IWRAP}(\theta, U_{10}, \phi)}{\partial \theta} \right|_{\theta=42^\circ} \quad (11)$$

for incidences  $\theta < 42^\circ$  such that

$$CPR(\theta, U_{10}, \phi) \Big|_{\theta_c < \theta < 42^\circ} \leq CPR_{Mouche}(\theta, \phi) \quad (12)$$

Based on the empirical data available and a reasonable use of physically-based upper and lower bounds, our best guess for HH GMF is constructed using the CMOD5.N VV GMF for winds from 4 to 65 m/s and incidence angles from 20 to 65 degrees, together with the extended VV to HH co-polarization model defined as above. The final results are shown in Figs. 11-16.

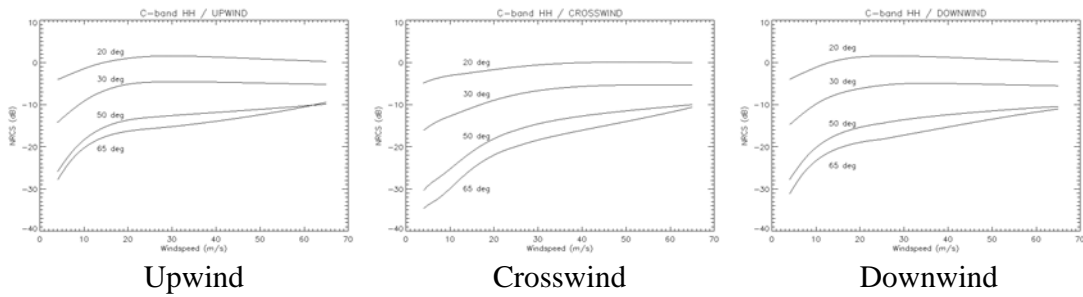


**Fig. 11** - CMOD5.N based C-band HH backscatter as a function of wind speed.

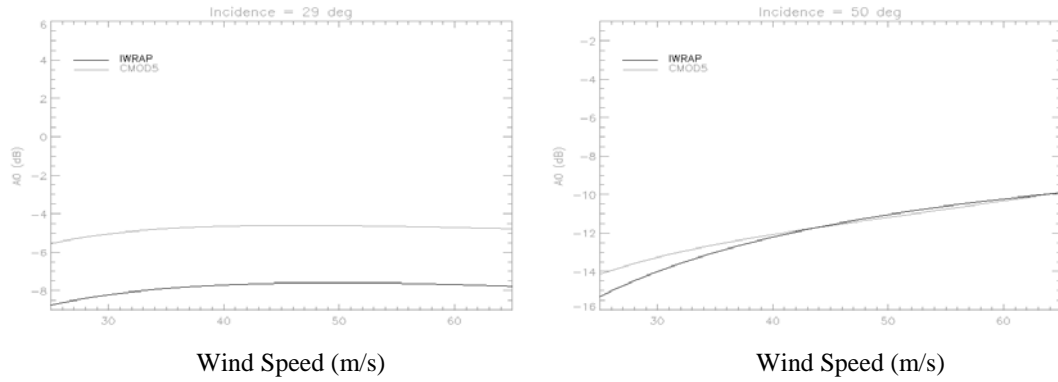


**Fig.12** – CMOD5.N and IWRAP isotropic B0 term (HH) as a function of wind speed at 29 and 50 deg incidence.

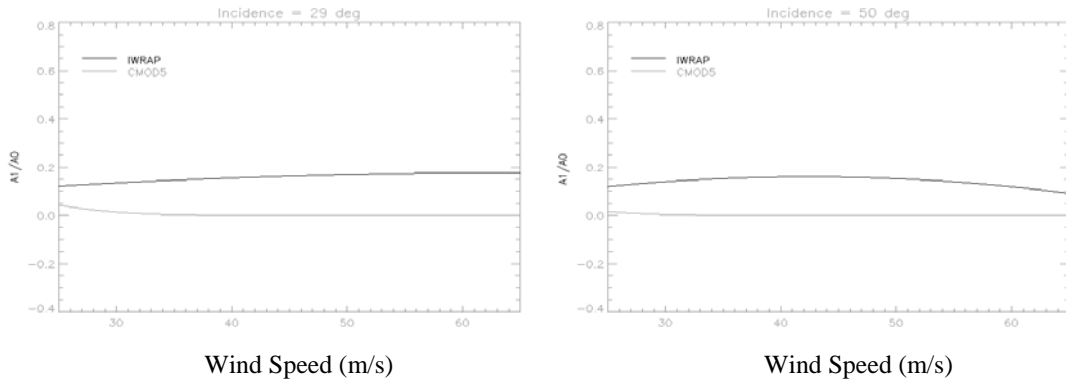


**Fig.13** – CMOD5.N and IWRAP up/downwind B1 term (HH) as a function of wind speed at 29 and 50 deg incidence.

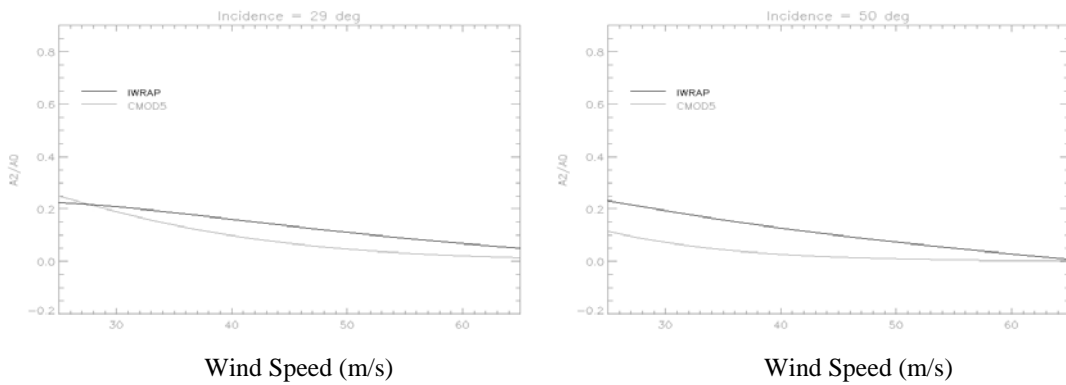


**Fig.14** – CMOD5.N and IWRAP up/crosswind B2 term (HH) as a function of wind speed at 29 and 50 deg incidence.

In general, the ocean backscatter at HH polarization is lower than VV by 1 to 4 dBs, with differences that increase at low winds and high incidence angles. HH polarized backscatter is also

characterized by increased sensitivity to high wind speeds at large incidence angles. Like its VV counterpart, C-band HH backscatter has low sensitivity to ocean winds at low incidence angles.

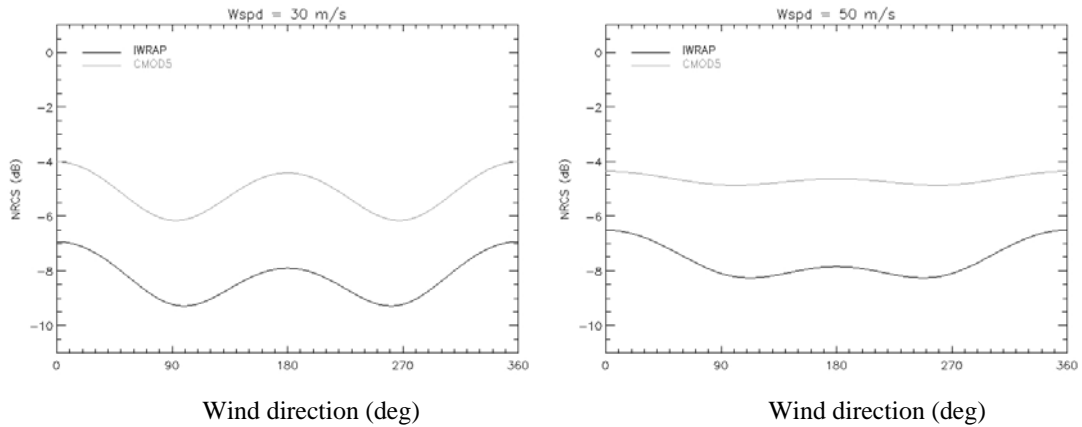


**Fig.15** – CMOD5.N and IWRAP C-band HH backscatter at 29 deg incidence (left 30 m/s, right 50 m/s)

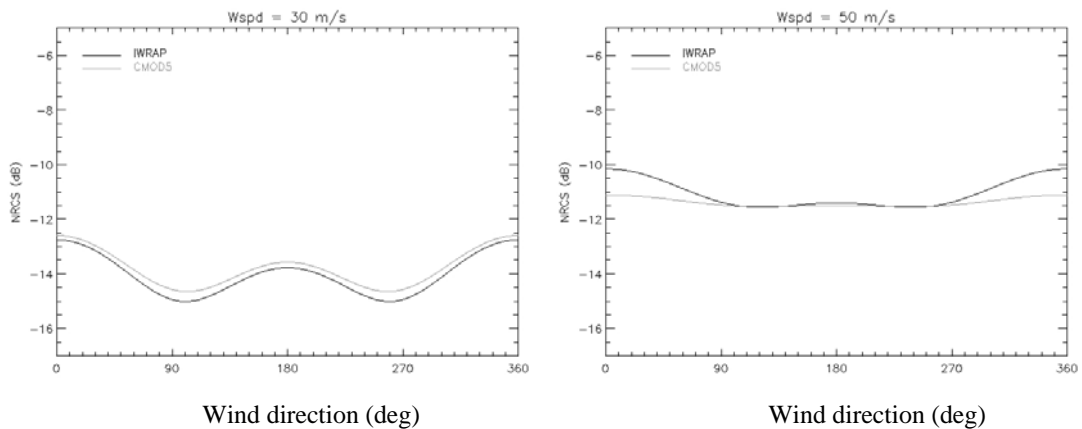


**Fig.16** – CMOD5.N and IWRAP C-band HH backscatter at 50 deg incidence (left 30 m/s, right 50 m/s)

### 2.3 - VH polarization GMF

Empirical GMFs for cross-polarized VH backscatter from the ocean at C-band (i.e. vertical polarization in transmit and horizontal in receive) has been estimated by [Hwang, 2010] and [Vachon, 2011] using cross-polarized RADARSAT-2 data. Both these studies indicate that VH backscatter depends very weakly on incidence angle and wind direction, and shows no signs of saturation at high wind speeds (unlike the co-polarized HH and VV returns, which show a saturation trend that starts at the lower incidence angles). From least squares fitting, the following empirical relation is proposed for wind speed inversion in the 0-20 m/s range and incidence angles from 20 to 41 deg [Hwang, 2010]:

$$U_{10} = H_1 \cdot (\sigma_{HV,dB}^0)^2 + H_2 \cdot \sigma_{HV,dB}^0 + H_3 \quad (13)$$

Inversely,

$$\sigma_{HV,dB}^0(U_{10}) = \left( -H_2 + \sqrt{H_2^2 - 4H_1(H_3 - U_{10})} \right) / (2H_1) \quad (14)$$

**Table 2** – Coefficients  $H_1$ ,  $H_2$ ,  $H_3$  for the  $\sigma_{VH}^0$  model of [Hwang, 2010]

	$H_1$	$H_2$	$H_3$
$\theta < 30$	$5.1178 \times 10^{-3}$	1.6664	54.235
$\theta > 30$	$-2.6444 \times 10^{-2}$	$-1.3433 \times 10^{-2}$	33.106

An alternative but more simple formulation, valid for incidence angles from 20 to 50 degrees and wind speeds from 0 to 20 m/s, is given by [Vachon, 2011]:

$$\sigma_{HV,dB}^0(U_{10}) = 0.592 \cdot U_{10} - 35.6 \quad U_{10} < 20 \text{ m/s} \quad (15)$$

The empirical relations in Eqs. (13) and (15) are plotted in Fig.17 below. They may be inverted trivially to permit estimation of wind speed from the observed C-band ocean VH backscatter, provided that the actual wind brings the signal sufficiently above the instrumental noise floor.

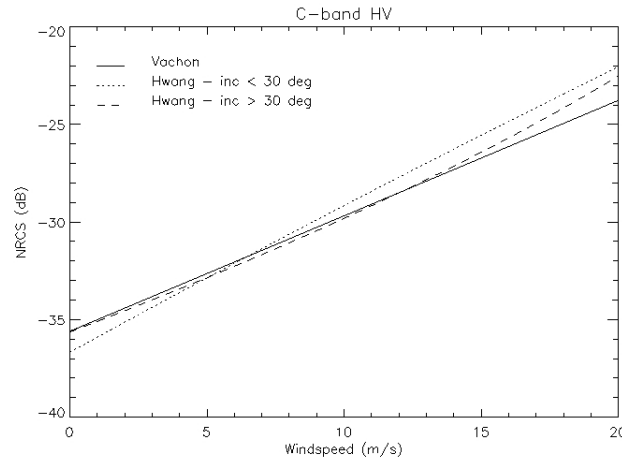


**Fig. 17** – [Vachon, 2011] and [Hwang, 2010] C-band VH backscatter models as a function of wind speed

The shape of the GMF for VH polarized backscatter at wind speeds larger than 20 m/s and its sensitivity to incidence angle and wind direction has been determined by [Zadelhoff, 2012] in the

light of new data collected over a number of tropical hurricanes. These data, which include RADARSAT-2 VH and VV backscatter measurements collected at 20 to 50 degrees of incidence and collocated against SFMR winds [Ulhorn, 2007] and ECMWF analyses, indicate that the VH GMF can be written as a function of wind speed and incidence angle as:

$$\sigma_{HV,dB}^0(U_{10}, \theta) = 0.163 \cdot U_{10} - 26.0 + \Delta dB(U_{10}, \theta) \quad U_{10} > 20 \text{ m/s} \quad (16)$$

With an incidence angle correction expressed as:

$$\Delta dB(U_{10}, \theta) = A_1 \cdot (\theta - \theta_0) + A_2 \cdot (\theta^2 - \theta_0^2) + U_{10} \cdot [B_1 \cdot (\theta - \theta_0) + B_2 \cdot (\theta^2 - \theta_0^2)]$$

$$\theta_0 = 30^\circ$$

$$A_1 = -0.654$$

$$A_2 = 8.94 E-3$$

$$B_1 = 4.38 E-2$$

$$B_2 = -6.35 E-4$$

The final VH GMF composite is formed letting the backscatter models expressed in Eq. 15 and Eq. 16 transition around 20 m/s as illustrated in Fig. 18. Note that the maximum sensitivity of the VH GMF to wind speed arises at mid-inner incidence angles (30-40 degrees), and that this sensitivity degrades notably over the mid-outer swath (more than 50 degrees).

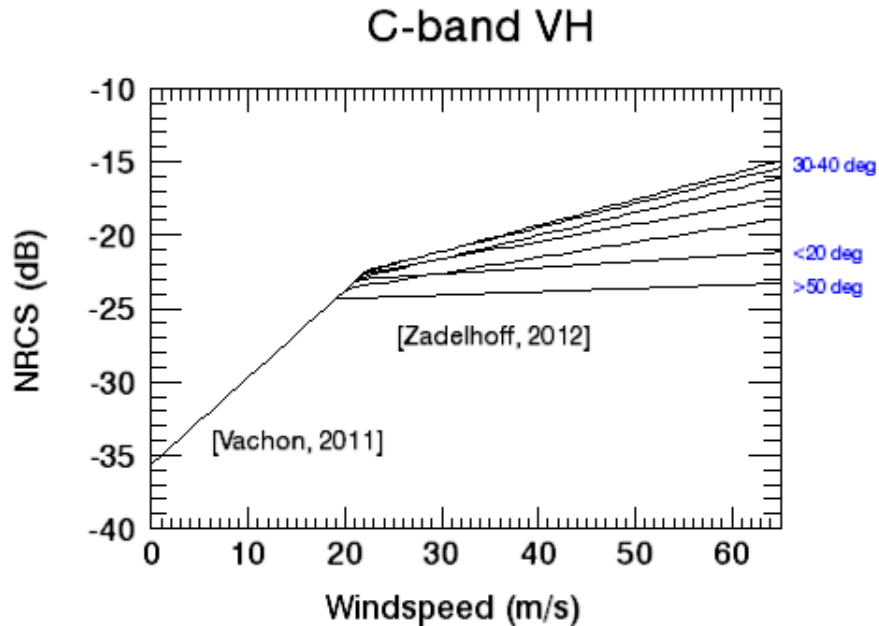


**Fig. 18** – Composite C-band VH backscatter model as a function of wind speed and incidence angle

Finally, simulation results indicate that a fully polarimetric system (with vertical or horizontal polarization in transmit, and both horizontal and vertical polarization in receive; it is the correlation between co- and cross-polarized returns that provides information in this case) could improve wind performance in the nadir region and eliminate the reliance on the external wind information necessary for ambiguity removal [Tsai, 2000]. The cross-polarization ratio would be required in order to quantify the SNR in the correlation of co- and cross-polarized returns for a fully polarimetric system, but this (costly) option has not been pursued during the EPS-SG scatterometer Phase 0 studies.

### 3 – Simulation and wind retrieval performance

The merit of a particular antenna/polarization configuration can be appraised after considering a number of performance metrics that include the dispersion of the output wind vector about the true wind (wind vector RMS or VRMS) using an *a priori* NWP wind condition, and the dispersion of the output wind magnitude about the true wind speed (wind speed RMS or WSRMS) regardless of wind direction.

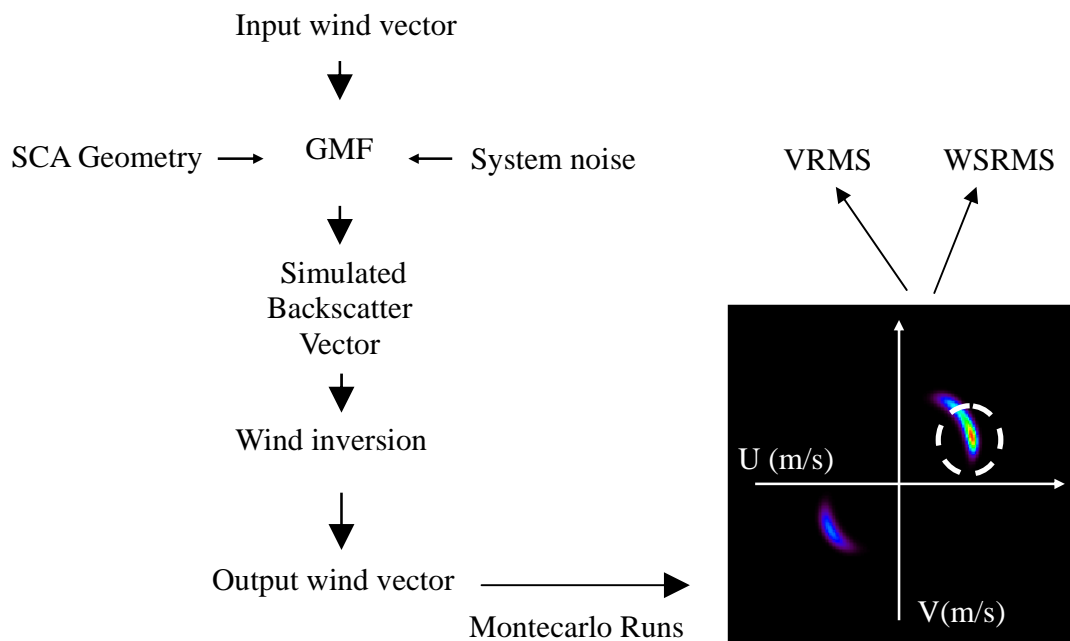


**Fig. 19** – End-to-end performance simulation

The true wind is input to an end-to-end simulator [Belmonte Rivas, 2010] that synthesizes a clean backscatter vector based on the observation geometry of the scatterometer and a Geophysical Model Function. The synthetic backscatter vector is corrupted by system noise, including the scatterometer instrumental (detector plus fading) noise but excluding geophysical noise – only considered relevant at low winds. It is assumed that the noise-equivalent  $\sigma^0$  (NESZ) and the number of looks of all the polarization options are identical to those achieved by the baseline VV case (ASTRIUM ASF0 concept) during Phase 0. The synthetic backscatter vector is then fed into the wind retrieval core of the simulator to generate a wind output. This operation is repeated a number of 1000 times per wind speed unit (0-65 m/s), wind direction (0-360 degrees) and WVC (-1000 to 1000 km across the scatterometer swath) to obtain an array of output wind probabilities  $P_{\text{obs}}(\mathbf{V}_{\text{out}}|\mathbf{V}_{\text{in}}, \text{WVC})$  such as displayed in Fig.19, which illustrates the dispersion of wind solutions about the input (true) wind for a given wind vector and across-track location. Using the wind output probabilities, it is then straightforward to calculate performance metrics such as:

$$\begin{aligned}
 VRMS(\bar{\mathbf{v}}_{\text{true}}, \text{WVC}) &= \left( \int |\bar{\mathbf{v}} - \bar{\mathbf{v}}_{\text{true}}|^2 P_{\text{obs}}(\bar{\mathbf{v}}|\bar{\mathbf{v}}_{\text{true}}, \text{WVC}) P_{\text{NWP}}(\bar{\mathbf{v}} - \bar{\mathbf{v}}_{\text{true}}) d^2 \mathbf{v} \right)^{1/2} \\
 WSRMS(\bar{\mathbf{v}}_{\text{true}}, \text{WVC}) &= \left( \int (|\bar{\mathbf{v}}| - |\bar{\mathbf{v}}_{\text{true}}|)^2 P_{\text{obs}}(\bar{\mathbf{v}}|\bar{\mathbf{v}}_{\text{true}}, \text{WVC}) d^2 \mathbf{v} \right)^{1/2}
 \end{aligned} \tag{17}$$

The *a priori* NWP wind condition  $P_{\text{NWP}}(\mathbf{v} - \mathbf{v}_{\text{true}})$  is a Gaussian function centered about the true wind with a standard deviation of 3.2 m/s for  $U_{10} < 20$  m/s and 10 m/s for  $U_{10} > 20$  m/s, reflecting a degraded knowledge of the *a priori* wind fields under high wind conditions. The first figure of merit, VRMS, refers to retrieval qualities of a given antenna configuration after imposing an *a priori* NWP wind condition – this figure is conditioned by the availability and reliability of the *a priori* wind field. The last figure of merit, WSRMS, relates to the retrieval of the wind magnitude (regardless of direction) in the absence of an *a priori* NWP wind condition.

### 3.1 – Proposed antenna configurations

The simulation strategy for testing the introduction of HH and VH capabilities to the baseline EPS-SG scatterometer concept defined in Phase 0 is shown in Figure 20. Simulations are carried out in support of Phase A for the following antenna configurations:

- A) VV on all beams with addition of VH on all beams

- B) VV on all beams with addition of VH on Fore and Aft beams
- C) VV on all beams with addition of VH on mid beam
- D) HH on all beams
- E) HH on all beams with substitution of VV in mid beam
- F) HH on all beams with substitution of VV on Fore and Aft beams

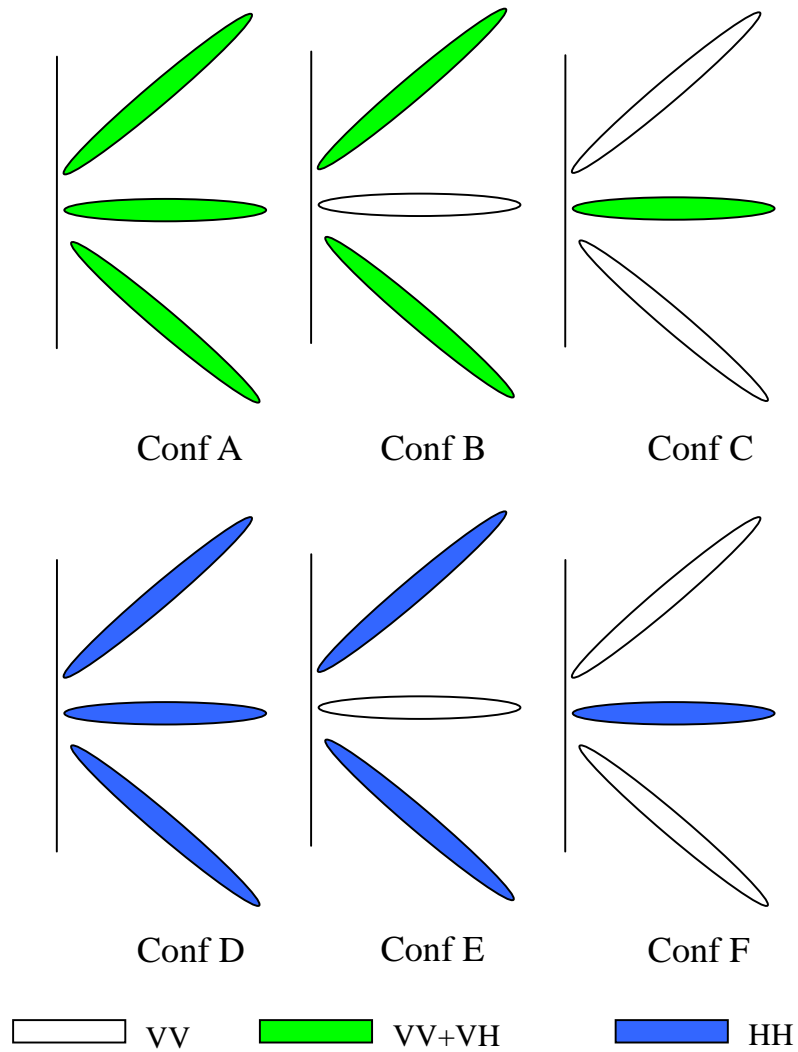


**Fig. 20** – Proposed antenna configurations

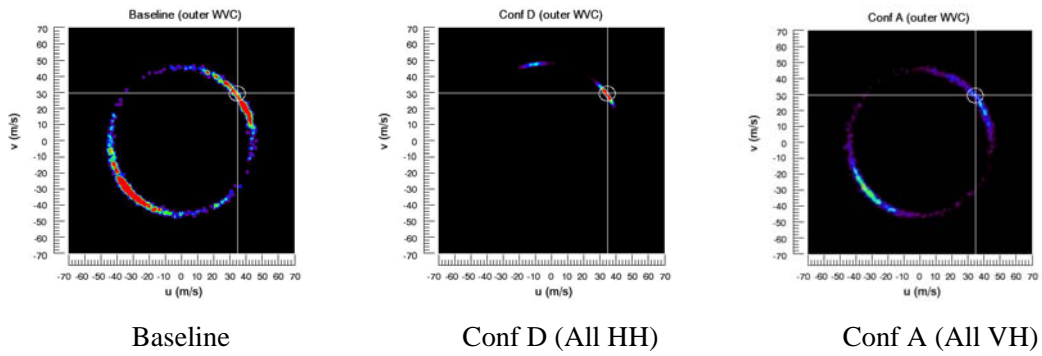
Because the baseline EPS-SG scatterometer can accommodate both VV and VH beams simultaneously in transmit/receive, but not VV and HH, the VH capability is added to the existing baseline VV beam, while HH capabilities replace VV beams where indicated.

## 3.2 – Simulation results

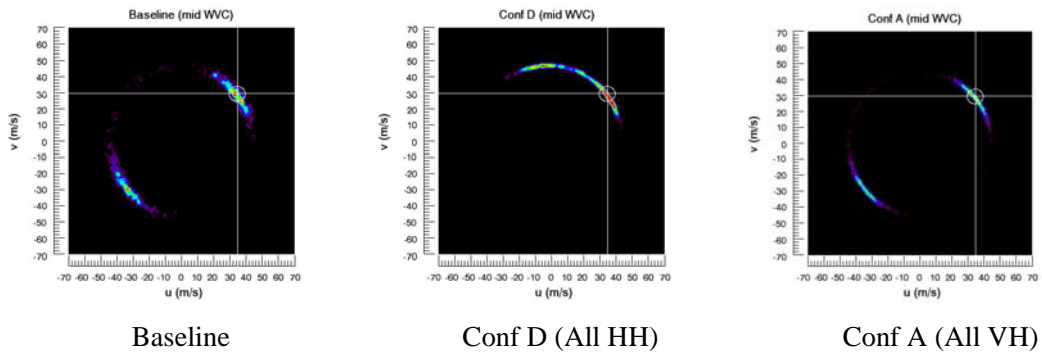
### Wind Vector RMS (VRMS)

Figure 23 shows the VRMS metric averaged over wind direction at discrete wind levels: 10, 25, 45 and 65 m/s for all the configurations under study and the baseline EPS-SG scatterometer results plotted in black for reference. At 10 m/s, only configurations A and B seem to perform worse than baseline. At 25 m/s, none of the proposed configurations looks much different from the others in terms of VRMS. At higher wind speeds, 45 and 65 m/s, the relative strengths of the different configuration families start to take form. The HH GMF is characterized by enhanced sensitivity to high wind speeds at high incidence angles, so that HH configurations tend to do better over outer swath cells. The sensitivity of the VH GMF to high winds is better at lower incidence angles (see Fig. 18), so that VV+VH configurations tend to perform better over inner swath cells.

To characterize these relative strengths in more detail, we examine the output wind probabilities  $P_{\text{obs}}(V_{\text{out}}|V_{\text{in}}, \text{WVC})$  that result after using a fixed input wind  $V_{\text{in}}$  (45 and 65 m/s at 45 degrees) and three different across-locations (inner, mid and outer WVCs at 260, 580 and 900 km from the sub-satellite track) in Figs. 21 and 22. These plots support the following rule: at high winds and in the presence of a NWP first guess, HH configurations (here represented by configuration D) perform better over *outer swath* cells than VV+VH configurations (here represented by configuration A). An example of this is shown in Figs. 21\_outer and 22\_outer. The reverse holds true over inner swath cells, where VV+VH configurations perform better than HH configurations. An example of this is shown in Figs. 21\_inner and 22\_inner. In terms of VRMS, the situation remains somewhat ambiguous across the mid swath (see Figs. 21\_mid and 22\_mid), where a directional but skewed HH configuration contends against an unbiased but more adirectional VH retrieval. Simulation results at extreme high winds (65 m/s) provide a very similar picture, which we summarize as this: the baseline EPS-SG scatterometer design features a large dispersion in the retrieved wind magnitude and finds it difficult to resolve wind direction across the entire swath. The ability to retrieve wind direction is improved by introducing HH beams, particularly over the outer swath. The ability to determine the wind magnitude is improved by introducing VH beams, particularly over the inner swath and for the mid beam (Conf C/F).



**Fig. 21\_outer** – Output wind probabilities at 45 m/s and outer swath: HH performs better than VH



**Fig. 21\_mid** – Output wind probabilities at 45 m/s and mid swath WVC: HH and VH are contested

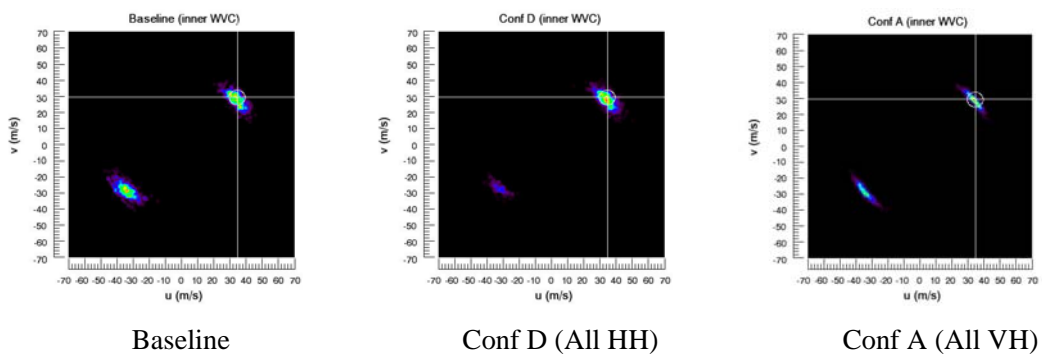


**Fig. 21\_inner** – Output wind probabilities at 45 m/s and inner swath: VH performs better than HH

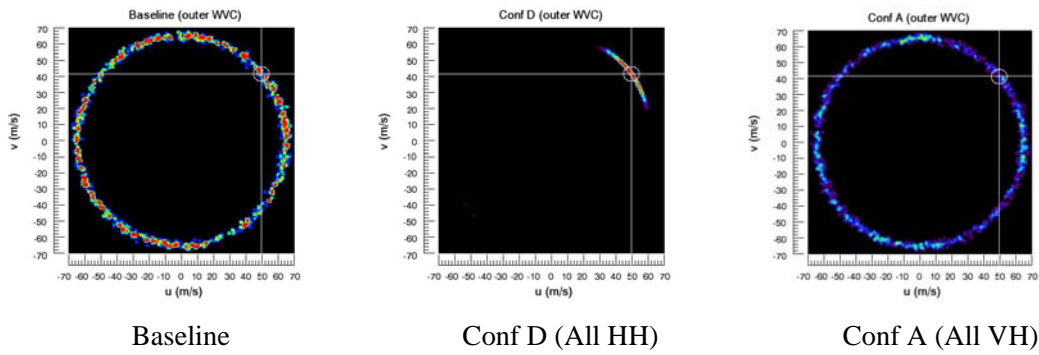


**Fig. 22\_outer** – Output wind probabilities at 65 m/s and outer swath: VH performs better than HH

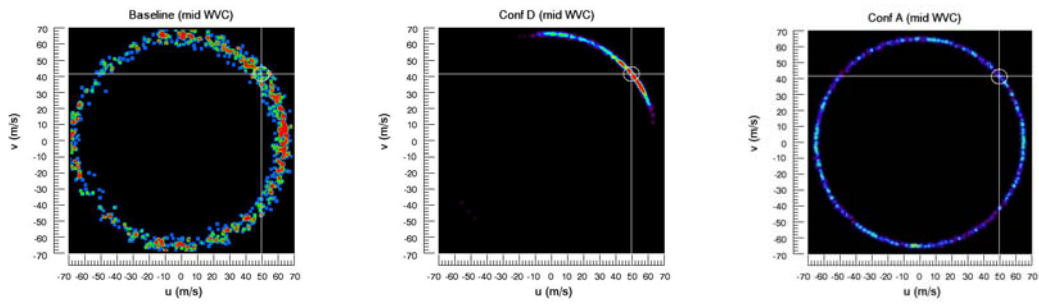


**Fig. 22\_mid** – Output wind probabilities at 65 m/s and mid swath: HH and VH are contested

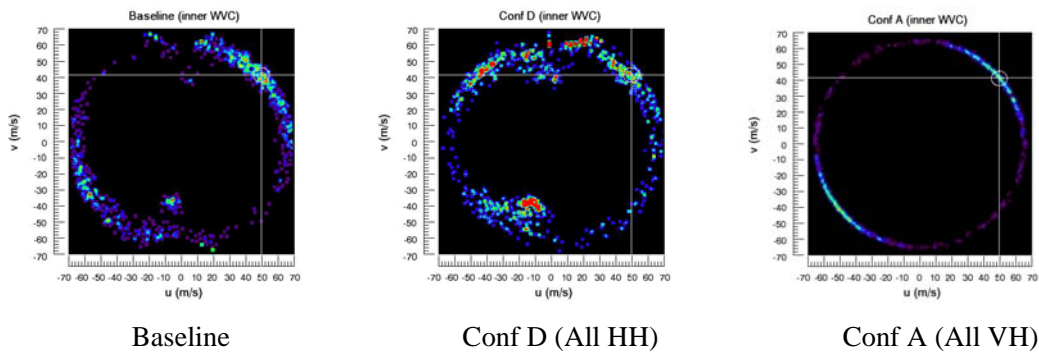


**Fig. 22\_inner** – Output wind probabilities at 65 m/s and inner swath: VH performs better than HH

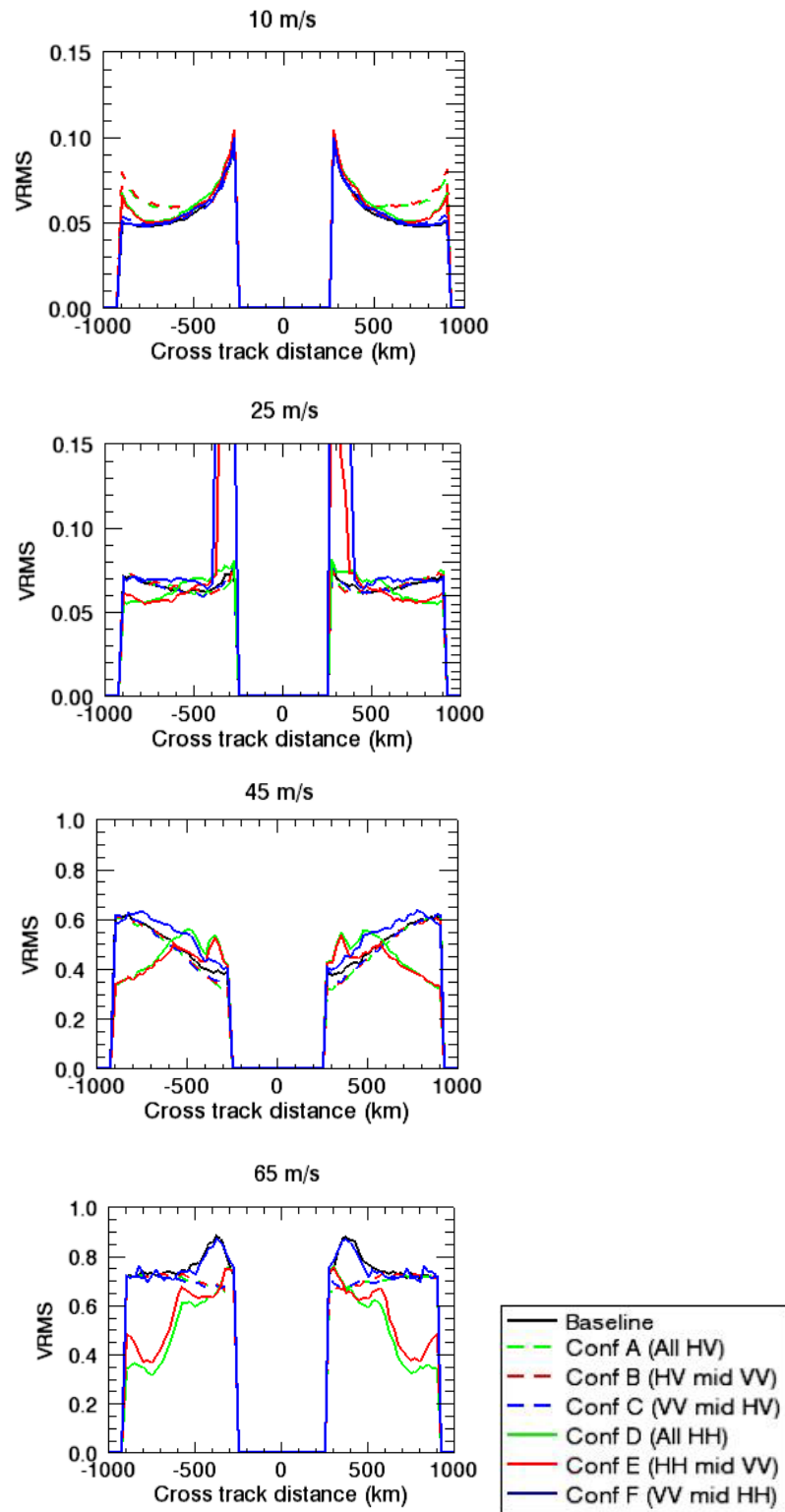


**Fig. 23** – Comparison of VRMS at 10, 25, 45 and 65 m/s

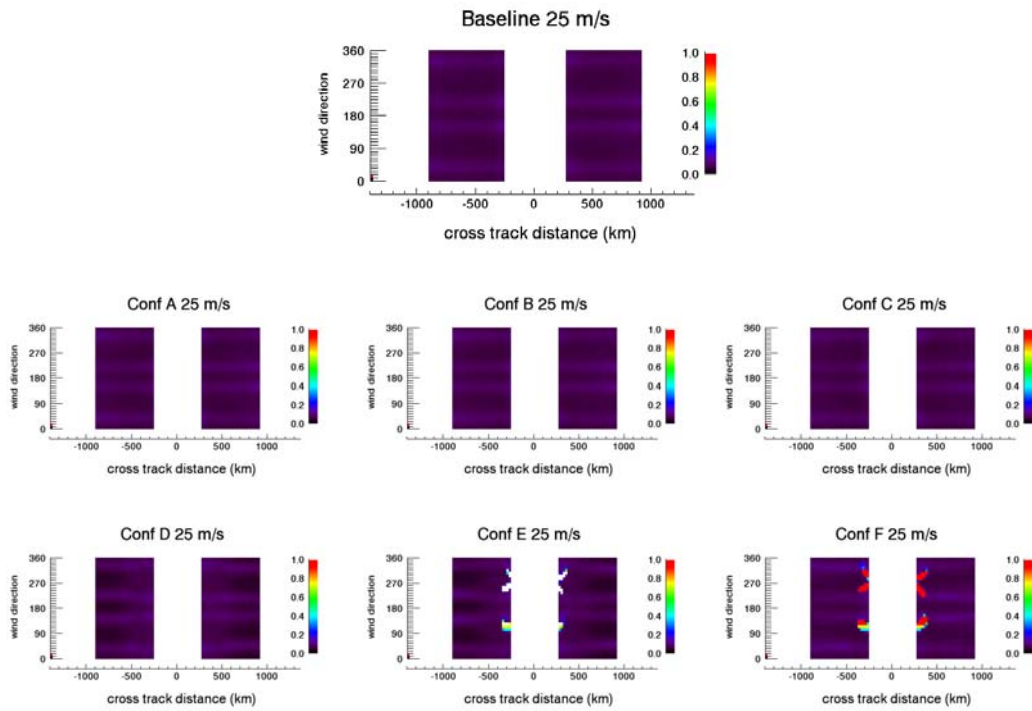


**Fig. 24** – Comparison of VRMS at 25 m/s: dependence on input wind direction

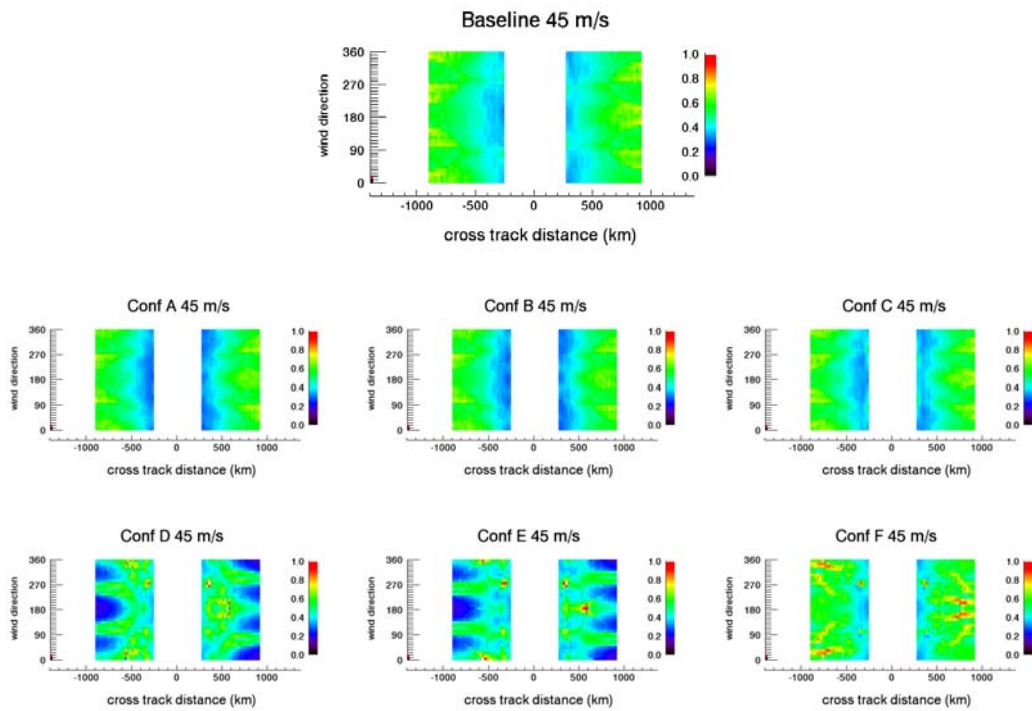


**Fig. 25** – Comparison of VRMS at 45 m/s: dependence on input wind direction

Figures 24 and 25 take a closer look at the behavior of the VRMS metric for different input wind directions at 25 and 45 m/s. While nothing extraordinary seems to happen at 25 m/s, Figure 25 makes clear the fact that adding a VH capability to the baseline EPS-SG scatterometer results in uniformly better inner swath retrievals at high winds. The advantage in replacing VV with HH beams is felt mainly in the outer swath (requires at least two HH beams) but less uniformly so, showing a degraded performance for winds blowing at 90, 180 and 270 degrees (i.e. along track and across-track).

### Wind Speed RMS (WSRMS)

The lack of sensitivity of the VV, HH or VH GMFs to wind direction at extreme high winds produces retrievals that depend heavily on external NWP information for the determination of wind direction. This particularity supports the definition a new performance figure that measures the accuracy in wind magnitude, regardless of skill in the determination of wind direction. In this scenario, the determination of wind direction is considered irrelevant – or inferable from means extraneous to the scatterometer. Figure 26 shows the wind speed RMS error (WSRMS) metric averaged over wind direction at discrete wind levels: 10, 25, 45 and 65 m/s for all the configurations under study. The different antenna configurations have been color coded differently, and the baseline EPS-SG scatterometer results plotted in black for reference. At 10 m/s, configuration D stands out with the largest WSRMS error, likely caused by HH backscatter being lower than VV in the domain of low to moderate winds. At higher wind speeds, VH configurations clearly provide the best overall scores, with an uneven distribution of WSRMS performance over the swath. Because of the better sensitivity of the VH GMF to wind speeds at lower incidence angles, the VH configurations that hold the VH beams at lower incidence angles on the ground (configurations A and C) provide the best scores within the VH family. Figures 27 and 28 examine the behavior of the WSRMS metric for all configurations as a function of input wind direction at 25 and 45 m/s. The HH configurations suffer from large WSRMS anomalies in the inner swath and along the same azimuthal angles that afford the best retrievals of wind direction. In contrast, VH configurations perform uniformly well across input wind directions and over large ranges of incidence, with better performance over inner to mid swath WVC cells.

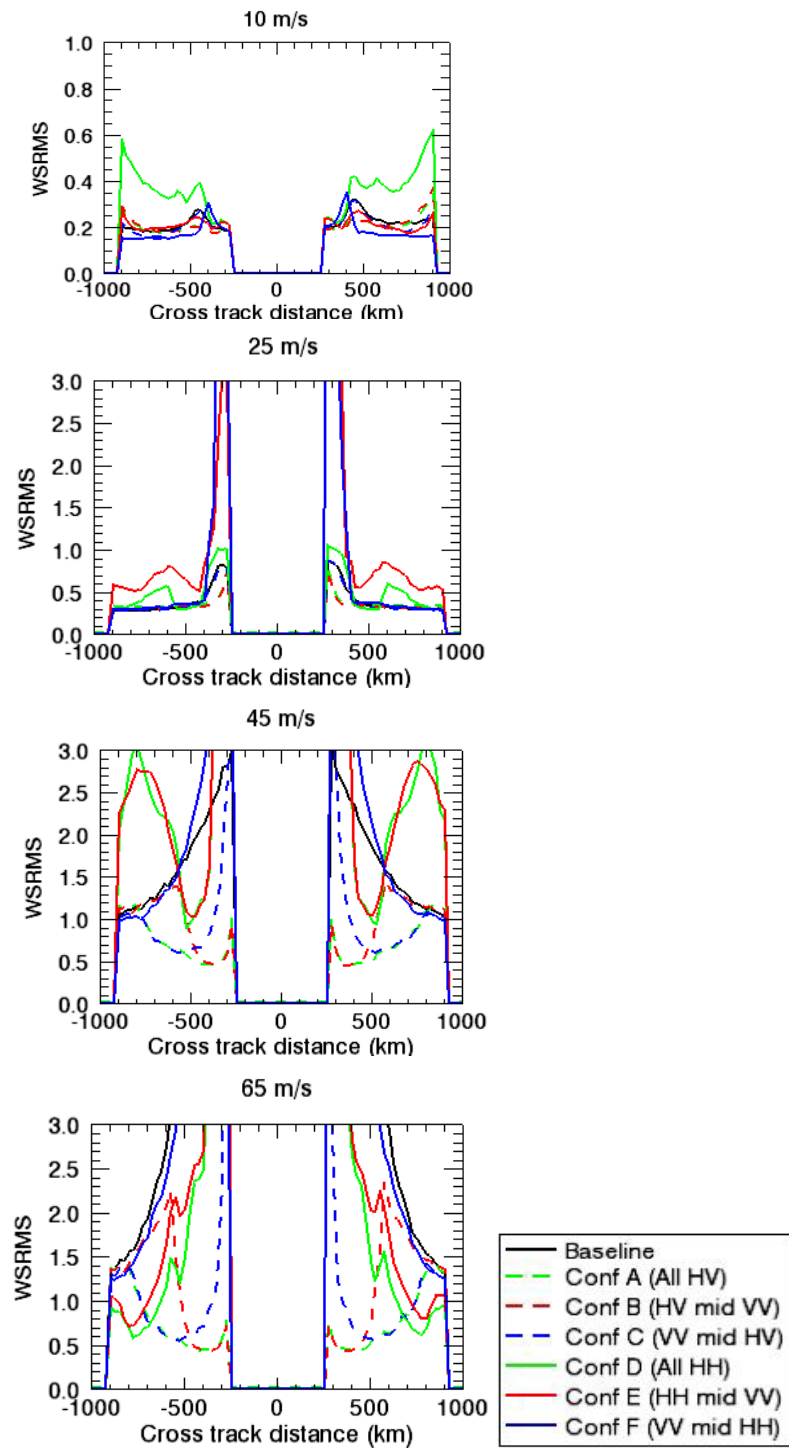


**Fig. 26** – Comparison of WSRMS at 10, 25, 45 and 65 m/s

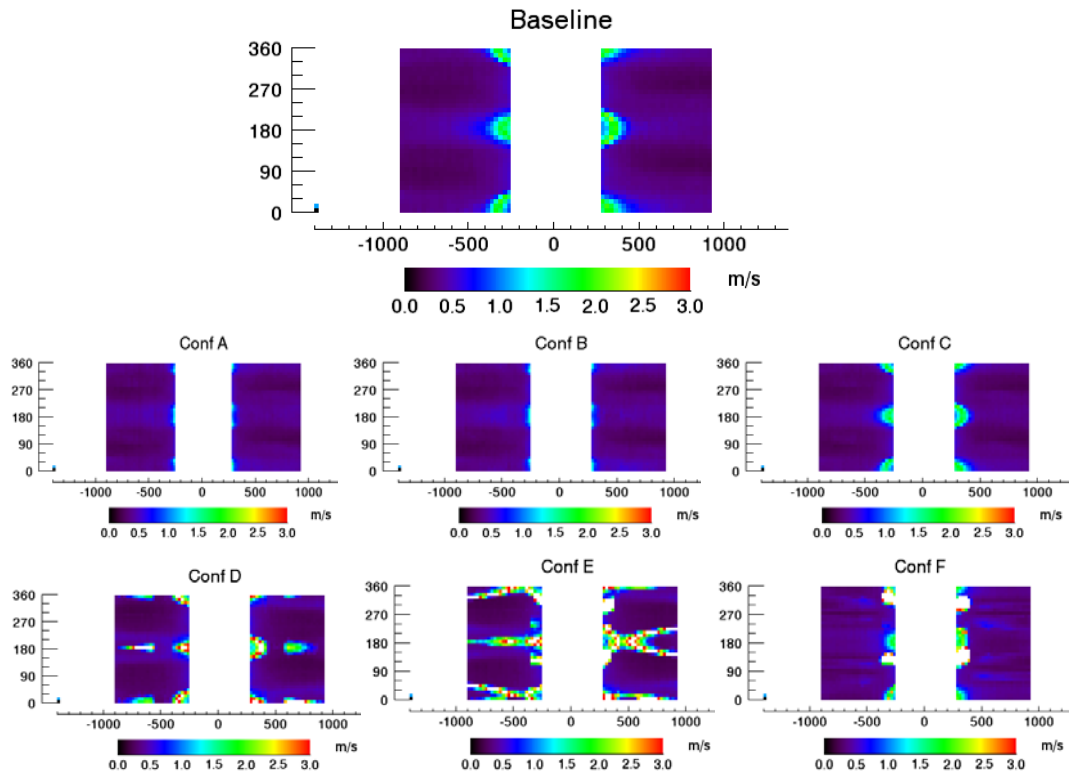


Fig. 27 – Comparison of WSRMS at 25 m/s: dependence on wind direction

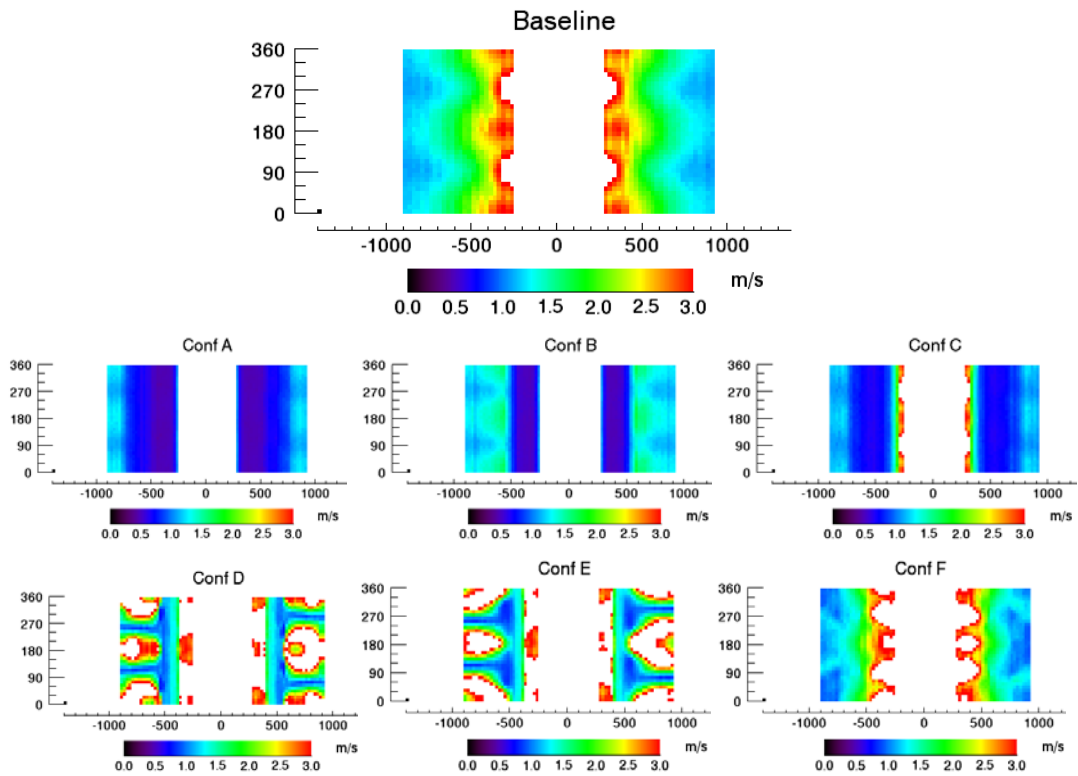
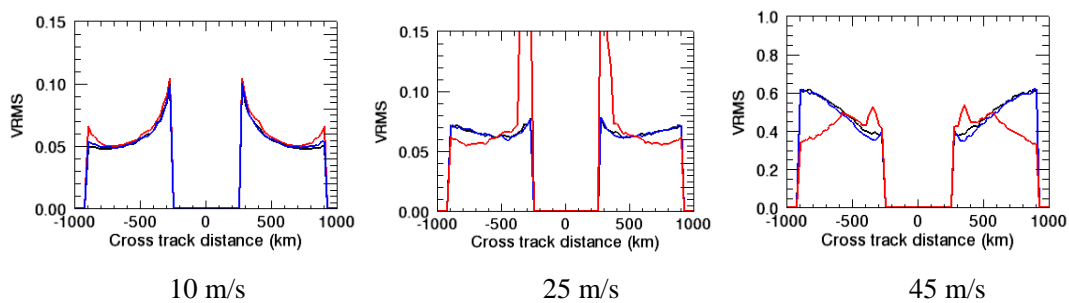


Fig. 28 – Comparison of WSRMS at 45 m/s: dependence on wind direction

### 3.3 - Discussion

While it is difficult to discriminate the merits afforded by the different polarization options, the matter can be simplified by elimination of all those configurations that show undesirable properties. For example, configuration A gives the best WSRMS scores at high wind speeds, but its VRMS score in the nominal range of 10 m/s is worse than baseline, so it can be discarded. Configuration B has a worse VRMS than baseline at 10 m/s and the worst WSRMS at high winds within the VH family, so it can be discarded too. Configuration D provides the best VRMS scores at high wind speeds, but its WSRMS score at 10 m/s is worse than baseline, so it can be discarded. Of all the HH configurations, the only one that does not provide good VRMS scores at high winds is configuration F, so it can be discarded also. That leaves only two candidates with overall good properties both in the nominal and extreme high wind speed domains, namely configuration C (all VV beams with VH added in the middle antenna) and configuration E (all HH beams with VV replacing the middle antenna). The following figures summarize their merits and relative performance.



**Fig. 29** – Comparison of best VRMS at 10, 25 and 45 m/s: configuration C (blue) and configuration E (red)

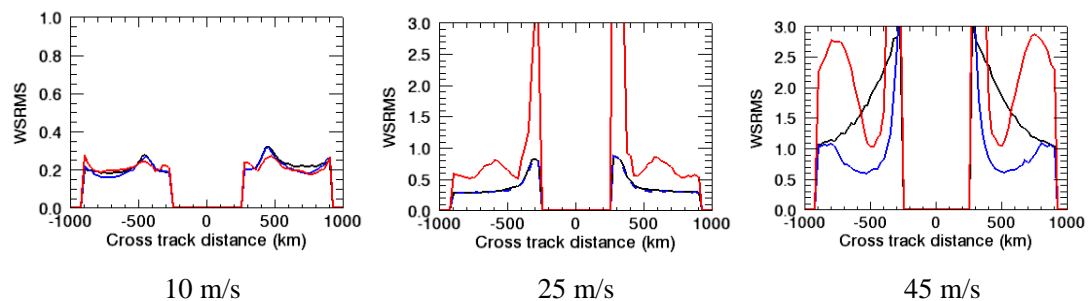
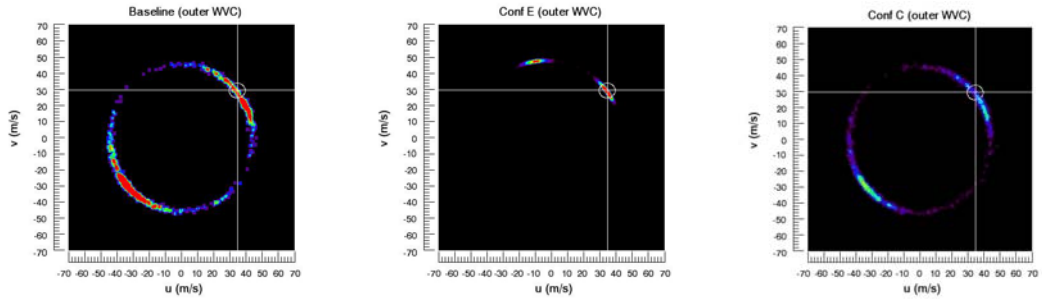


**Fig. 30** – Comparison of best WSRMS at 10, 25 and 45 m/s: configuration C (blue) and configuration E (red)

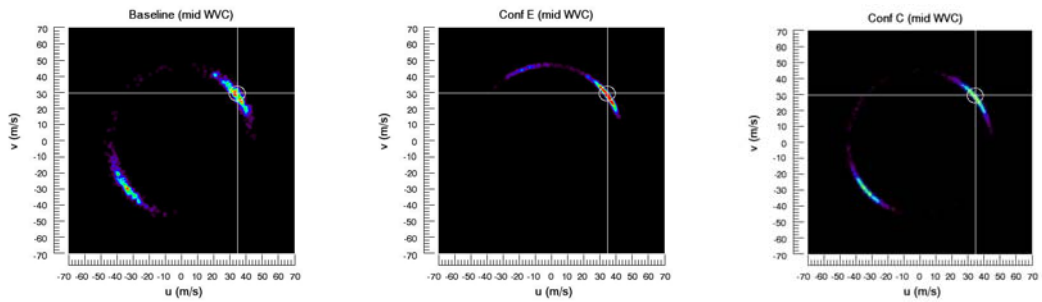


Baseline

Conf E (HH mid VV)

Conf C (VV mid VH)

**Fig. 31\_outer** – Output wind probabilities at 45 m/s and outer swath (900 km across-track)

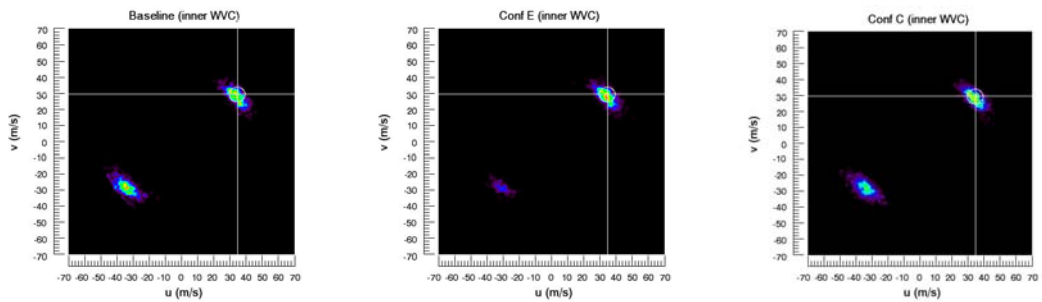


Baseline

Conf E (HH mid VV)

Conf C (VV mid VH)

**Fig. 31\_mid** – Output wind probabilities at 45 m/s and mid swath (580 km across-track)



Baseline

Conf E (HH mid VV)

Conf C (VV mid VH)

**Fig. 31\_inner** – Output wind probabilities at 45 m/s and inner swath (260 km across-track)

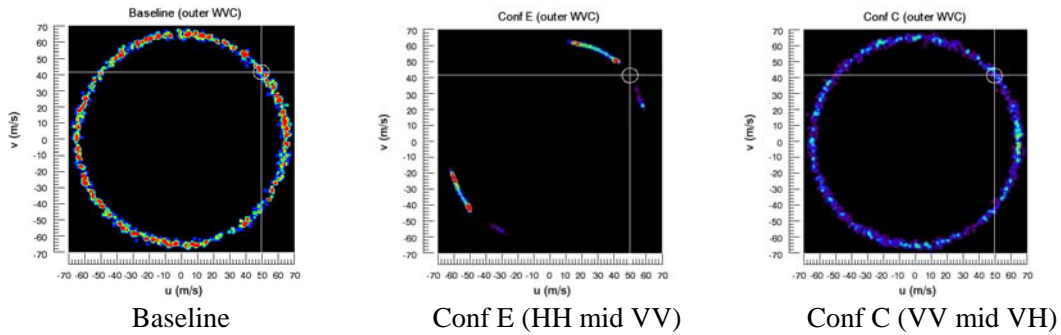


**Fig. 32\_outer** – Output wind probabilities at 65 m/s and outer swath (900 km across-track)

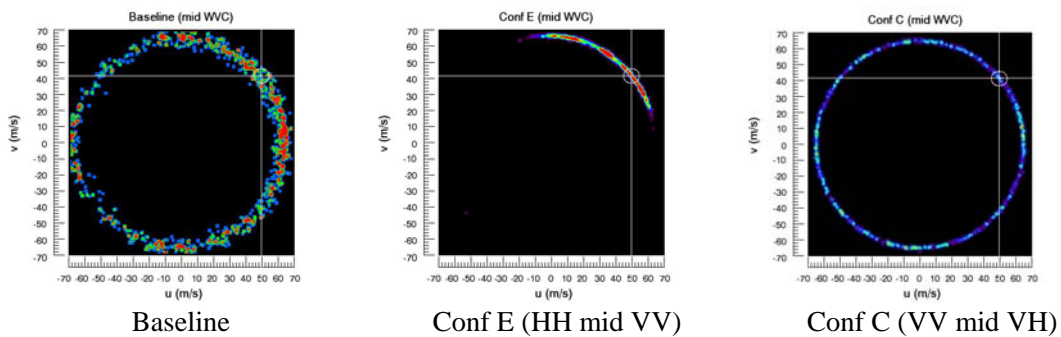


**Fig. 32\_mid** – Output wind probabilities at 65 m/s and mid swath (580 km across-track)

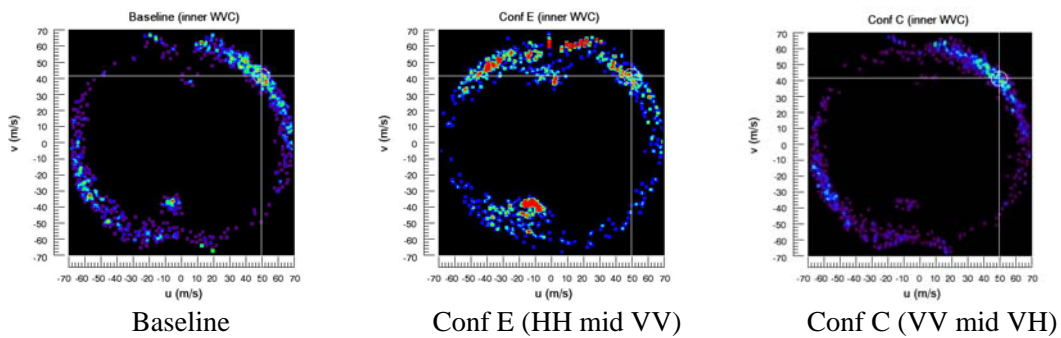


**Fig. 32\_inner** – Output wind probabilities at 65 m/s and inner swath (260 km across-track)

The relative strengths of the two best candidates are directly inherited from their respective HH (Conf E) and VH (Conf C) families. Configuration E features better wind direction retrieval properties, particularly over the outer swath, whereas configuration C affords a better determination of the wind magnitude across mid swath cells. In the light of this information, it may be possible to conciliate the best of both polarization options by combining them into a composite configuration that holds HH beams in the fore/aft antennas and a VV+VH capability in the mid antenna, as illustrated in Fig. 33. In this manner, their relative strengths merge into a

single system that operates nominally at low to moderate winds (0-25 m/s) and optimally in the extreme high wind speed range (25 to 65 m/s). The VH capability in the mid beam (with lowest possible incidence on the ground) provides an improved determination of the wind magnitude across most of the swath, the HH capability in the fore/aft beams (with highest possible incidence on the ground) affords an improved determination of wind speed and direction, especially for outer swath cells, and the VV capability in the mid beam compensates for the utilization of weaker -but more sensitive- HH signals, guaranteeing that the system behaves nominally in the low to moderate wind speed range.

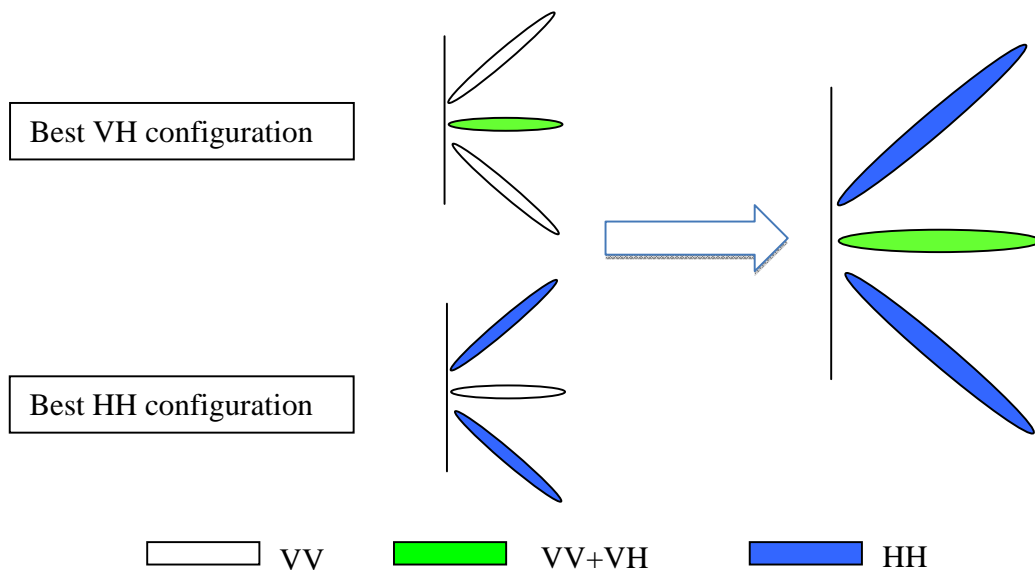


**Fig. 33** – Recommended antenna configuration for best performance at extreme wind speeds

## 5 – Conclusions

The utilization of the CMOD5.N GMF for VV polarized ocean backscatter at C-band is well justified over the entire incidence angle and wind speed range covered by the baseline EPS-SG scatterometer – with small discrepancies regarding the upwind/downwind asymmetry (<1dB) captured by IWRAP at winds over 50 m/s. The GMF for HH polarized backscatter is rooted on CMOD5.N VV GMF results for winds from 4 to 65 m/s and incidence angles from 20 to 65 degrees, and obtained through incorporation of an empirical model of the ocean co-polarization ratio that mimics RADARSAT-2 VV/HH observations at low incidence angles and IWRAP VV/HH observations at the higher incidence angles – the IWRAP VV/HH ratio at low incidence angles is found inconsistent with physical predictions and consequently discarded. The GMF for

VH backscatter is a simple linear function of wind speed at low winds, featuring a small dependence on incidence angle for winds larger than 20 m/s.

The performance of a suite of antenna configurations based on the baseline ASCAT-type EPS-SG scatterometer concept has been simulated using the VV, HH and VH geophysical model information described in the first part of this report. Our simulation results support the following general conclusions:

- The VH capability provides improved sensitivity to wind magnitude at high wind speeds across most of the swath, especially at low to mid incidence angles. This capability is best employed in a mid beam, so that the incidence on the ground is minimized. The VH capability is insensitive to wind direction, and provides much weaker backscatter signals than either VV or HH at low to moderate wind speeds.
- The HH capability provides improved sensitivity to wind speed and direction at high wind speeds, especially at large incidence angles. This capability is best employed in the fore/aft beams, where incidence on the ground becomes the largest. The HH capability affords weaker backscatter signals than VV at low to moderate winds – especially at high incidence angles.
- The VV capability provides stronger backscatter signals at low to moderate winds, particularly in the outer swath. Its utilization helps compensate for the utilization of weaker -but more sensitive- HH signals, guaranteeing that the system behaves nominally in the low to moderate wind speed range.

There is a limited number of polarization options that may improve wind retrievals under hurricane conditions without detriment to the nominal scatterometer operation at low to moderate winds. These options include the introduction of a VH capability in the mid-beam antenna, and the introduction of HH beams in the fore/aft antennas. The first option provides better sensitivity to wind magnitude at high winds over most of the swath. The second option provides better sensitivity to wind speed and direction at high winds, particularly over the outer swath. These two options are in no way excluding, and may operate alongside in a configuration that holds HH beams in the fore/aft antennas and a VV+VH capability in the mid antenna, as illustrated in Fig. 33. If the determination of wind direction at high winds is not an issue, then the introduction of a

single VH capability in the mid-beam antenna may arise as the most simple and cost-effective solution.

## References

- [Donnelly, 1999] Donnelly, W.J., Carswell, J.R., McIntosh, R.E., Chang, P.S., Wilkerson, J., “Revised ocean backscatter models at C and Ku-band under high wind conditions”, *J. Geophys. Res.*, 104(C5), 11,485-11497, 1999.
- [Belmonte Rivas, 2010] Belmonte Rivas, M., de Kloe, J., Stoffelen, A., “Study of an objective performance measure for spaceborne wind sensors”, ESA Contract 18041/04/NL/AR, 2010.
- [Esteban, 2006] Esteban-Fernandez, D., Carswell, J.R., Frasier, S., Chang, P.S., Black, P.G., Marks, F.D., “Dual-polarized C- and Ku-band ocean backscatter response to hurricane-force winds”, *J. Geophys. Res.*, Vol.111, C08013, 2006.
- [Hersbach, 2007] Hersbach, H., Stoffelen, A., de Haan, S., “An improved C-band scatterometer ocean geophysical model function: CMOD5”, *J. Geophys. Res.*, Vol.112, C03006, 2007.
- [Hwang, 2010] Hwang, P.A., Zhang, B., Toporkov, J.V., Perrie, W., “Comparison of composite Bragg theory and quad-polarization radar backscatter from RADARSAT-2: with applications to wave breaking and high wind retrieval”, *J. Geophys. Res.*, Vol. 115, C08019, 2010.
- [Lin, 2011] Lin, C.C., Betto, M., Belmonte Rivas, M., Stoffelen, A., De Kloe, J., “EPS-SG windscatterometer concept trade-offs and wind retrieval performance assessment”, *IEEE Trans. Geosc. Remote Sens.* (submitted), 2011.
- [Liu, 2000] Liu, C., Park, P., Stoffelen, A., Wismann, V., “Optimization of rotating, range-gated, fanbeam scatterometer for wind retrieval”, Task 1 Technical Report, ESA/ESTEC Contract No.:14383/00/NL/DC, 2000.

- [Mouche, 2005] Mouche, A., Hauser, D., Daloze, F., Guerin, C., “Dual-polarization measurements at C-band over the ocean: results from airborne radar observations and comparison with ENVISAT SAR data”, IEEE Trans. Geosci. Rem. Sens., Vol.43, No.4, pp 753-769, 2005.
- [Portabella, 2009] Portabella, M., Stoffelen, A.C.M, “On scatterometer Ocean Stress”, J. Atm. Oceanic Technol., Vol.26, No.2, pp 368-382, 2009.
- [Stoffelen, 1998] Stoffelen, A., “Scatterometry”, PhD Thesis, U. Utrecht, 1998.
- [Tsai, 2000] Tsai, W.Y., Nghiem, S.V., Huddleston, J.N., Spencer, M.W., Stiles, B., West, R., “Polarimetric scatterometry: a promising technique for improving ocean surface wind measurements from space”, IEEE. Trans. Geosci. Rem. Sens., Vol. 38, No.4, pp 1903-1921, 2000.
- [Ulhorn, 2007] Ulhorn, E.W., (et al.), “Hurricane surface wind measurements from an operational Stepped Frequency Microwave Radiometer”, Mon. Wea. Rev., 135, 3070-3085, 2007.
- [Vachon, 2011] Vachon, P.W., Wolfe, J., “C-band cross-polarization wind speed retrieval”, IEEE Geosci. Rem. Sens. Lett., Vol.8, No.3, 2011.
- [Zadelhoff, 2012] Zadelhoff, G.J., Stoffelen, A., Vachon, P., Wolfe, J., Belmonte Rivas, M., “Cross-polarization measurements on the ASCAT second generation”, Technical Report, SAF/OSI/CDOP/KNMI/TEC/RP/193, 2012.

## Appendix A – CMOD5 VV ocean backscatter model

The GMF for vertically polarized ocean wind backscatter CMOD5 is expressed in linear units as:

$$\sigma^0(\theta, U_{10}, \phi) = B_0(\theta, U_{10}) [1 + B_1(\theta, U_{10}) \cos \phi + B_2(\theta, U_{10}) \cos 2\phi]^{1.6} \quad (\text{A1})$$

Where  $\theta$  is the incidence angle in degrees,  $U_{10}$  the ocean wind speed at 10 m height in m/s, and  $\phi$  the azimuth angle of wind flow relative to the antenna beam in degrees ( $\phi = 0$  is upwind). The isotropic  $B_0$  term is expressed as:

$$B_0(\theta, U_{10}) = 10^{a_0 + a_1 U_{10}} f(a_2 U_{10}, s_0)^\gamma \quad (\text{A2})$$

Where

$$f(s, s_0) = \begin{cases} s_0^\alpha g(s_0) & , s < s_0 \\ g(s) & , s \geq s_0 \end{cases} \quad \text{and} \quad g(s) = 1/(1 + e^{-s}) \quad (\text{A3})$$

The functional coefficients for the  $B_0$  term are written as a function of  $x = (\theta - 40)/25$ :

$$\begin{aligned} a_0 &= c_1 + c_2 x + c_3 x^2 + c_4 x^3 \\ a_1 &= c_5 + c_6 x \\ a_2 &= c_7 + c_8 x \\ \alpha &= s_0 (1 - g(s_0)) \\ \gamma &= c_9 + c_{10} x + c_{11} x^2 \\ s_0 &= c_{12} + c_{13} x \end{aligned} \quad (\text{A4})$$

The upwind-downwind  $B_1$  term is expressed as:

$$B_1(\theta, v) = \frac{c_{14}(1+x) - c_{15} \cdot v \cdot [0.5 + x - \tanh(4(x + c_{16} + c_{17}v))]}{1 + e^{0.34(v - c_{18})}} \quad (\text{A5})$$

The upwind-crosswind  $B_2$  term is expressed as:

$$B_2(\theta, \nu) = (-d_1 + d_2 \nu_2) \cdot e^{-\nu_2} \quad (\text{A6})$$

Where

$$\nu_2 = \begin{cases} a + b(y-1)^n & , \quad y < y_0 \\ y & , \quad y > y_0 \end{cases} \quad \text{with} \quad y = \frac{U_{10} + \nu_0}{\nu_0} \quad \text{and} \quad \begin{cases} a = y_0 - (y_0 - 1)/n \\ b = 1/[n(y_0 - 1)^{n-1}] \end{cases}$$

$$y_0 = c_{19} \quad n = c_{20}$$

$$\nu_0 = c_{21} + c_{22}x + c_{23}x^2$$

$$d_1 = c_{24} + c_{25}x + c_{26}x^2$$

$$d_2 = c_{27} + c_{28}x$$

(A7)

The CMOD5 GMF 28 coefficients are given in Table A1:

**Table A1.** CMOD5 Coefficients  $c$  Calibrated on ECMWF First-Guess Winds, FGAT<sup>a</sup>

	$c$	Value	Sensitivity
$a_0$	$c_1$	-0.688	$\pm 0.010$
	$c_2$	-0.793	$\pm 0.011$
	$c_3$	0.338	$\pm 0.013$
	$c_4$	-0.173	$\pm 0.015$
$a_1$	$c_5$	0.0000	$\pm 0.0002$
	$c_6$	0.0040	$\pm 0.0002$
$a_2$	$c_7$	0.111	$\pm 0.0014$
	$c_8$	0.0162	$\pm 0.002$
$\gamma$	$c_9$	6.34	$\pm 0.02$
	$c_{10}$	2.57	$\pm 0.02$
	$c_{11}$	-2.18	$\pm 0.03$
$s_0$	$c_{12}$	0.400	$\pm 0.006$
	$c_{13}$	-0.60	$\pm 0.02$
	$c_{14}$	0.045	$\pm 0.009$
$b_1$	$c_{15}$	0.007	$\pm 0.002$
	$c_{16}$	0.33	$\pm 0.04$
	$c_{17}$	0.012	$\pm 0.002$
	$c_{18}$	22.0	$\pm 1.4$
	$c_{19}$	1.95	$\pm 0.02$
	$c_{20}$	3.00	$\pm 0.15$
$\nu_0$	$c_{21}$	8.39	$\pm 0.17$
	$c_{22}$	-3.44	$\pm 0.23$
	$c_{23}$	1.36	$\pm 0.3$
$d_1$	$c_{24}$	5.35	$\pm 0.06$
	$c_{25}$	1.99	$\pm 0.08$
	$c_{26}$	0.29	$\pm 0.09$
$d_2$	$c_{27}$	3.80	$\pm 0.03$
	$c_{28}$	1.53	$\pm 0.04$

<sup>a</sup>Error bars represent those variations that give rise to a maximal change in backscatter of 0.1 dB (e.g., half the observation error) when evaluated over all wind speeds between 0.5 and 50.0 m s<sup>-1</sup>, all wind directions, and all incidence angles in between 18. and 58. degrees.

The validity domain for this model is 20 to 65 degrees in incidence angle and 4 to 65 m/s in windspeed. The transfer from CMOD5 to CMOD5.N is effected as:

$$\sigma_{CMOD5.N}^0(\theta, U_{10N}, \phi) = \sigma_{CMOD5}^0(\theta, U_{10} + 0.7, \phi) \quad (\text{A8})$$



## Appendix B – IWRAP VV and HH ocean backscatter models

The IWRAP GMFs for vertically and horizontally polarized ocean wind backscatter are expressed in linear units as:

$$\sigma^0(\theta, U_{10}, \phi) = A_0(\theta, U_{10})[1 + a_1(\theta, U_{10}) \cos \phi + a_2(\theta, U_{10}) \cos 2\phi] \quad (\text{B1})$$

Where  $\theta$  is the incidence angle in degrees,  $U_{10}$  the ocean wind speed at 10 m height in m/s, and  $\phi$  the azimuth angle of wind flow relative to the antenna beam in degrees ( $\phi = 0$  is upwind). The isotropic  $A_0$  term is expressed as:

$$A_0(\theta, U_{10}) = 10^\beta U_{10}^{\gamma_1 + \gamma_2 \cdot a \log_{10}(U_{10})} \quad (\text{B2})$$

Where beta, gamma1 and gamma 2 are interpolated function of incidence angle, from Table B1.

**Table B1.1** – IWRAP VV polarization  $\beta$ ,  $\gamma_1$ ,  $\gamma_2$  coefficients

Incidence	29°	34°	40°	50°
$\beta$	-3.807	-4.631	-5.081	-6.931
$\gamma_1$	4.064	4.641	4.784	6.808
$\gamma_2$	-1.185	-1.300	-1.266	-1.903

**Table B1.2** – IWRAP HH polarization  $\beta$ ,  $\gamma_1$ ,  $\gamma_2$  coefficients

Incidence	31°	36°	42°	49°
$\beta$	-4.892	-5.689	-5.570	-5.886
$\gamma_1$	4.7275	5.2932	4.6925	4.5876
$\gamma_2$	-1.3598	-1.4401	-1.1496	-1.0355

The upwind-downwind and upwind-crosswind terms,  $a_1$  and  $a_2$ , are expressed as:

$$\begin{aligned} a_1(\theta, U_{10}) &= c_0(\theta) + c_1(\theta) \cdot U_{10} + c_2(\theta) \cdot U_{10}^2 \\ a_2(\theta, U_{10}) &= d_0(\theta) + d_1(\theta) U_{10} + d_2(\theta) \cdot U_{10} \cdot \tanh(U_{10} / d_3(\theta)) \end{aligned} \quad (\text{B3})$$

Where  $c_0$ ,  $c_1$  and  $c_2$  are interpolated functions of incidence angle, from Table B2. The coefficients  $d_0$ ,  $d_1$ ,  $d_2$  and  $d_3$  are also interpolated functions of incidence angle, from Table B3.

**Table B2.1** – IWRAP VV polarization  $c_0, c_1, c_2$  coefficients

Incidence	29°	34°	40°	50°
$c_0$	1.500E-2	-1.080E-2	-1.757E-1	-5.453E-1
$c_1$	3.917E-3	7.046E-3	1.515E-2	2.710E-2
$c_2$	-1.6595E-5	-4.6334E-5	-14.830E-5	-28.064E-5

**Table B2.2** – IWRAP HH polarization  $c_0, c_1, c_2$  coefficients

Incidence	31°	36°	42°	49°
$c_0$	7.030E-2	-1.083E-1	8.060E-2	-1.053E-1
$c_1$	3.093E-3	1.354E-2	4.091E-3	1.289E-2
$c_2$	-1.8011E-5	-13.004E-5	-3.5243E-5	-14.723E-5

**Table B3.1** – IWRAP VV polarization  $d_0, d_1, d_2$  and  $d_3$  coefficients

Incidence	29°	34°	40°	50°
$d_0$	6.021E-2	-4.288E-2	1.972E-1	1.291E-1
$d_1$	1.904E-2	6.199E-2	2.561E-2	3.551E-2
$d_2$	-2.026E-2	-6.066E-2	-2.837E-2	-3.714E-2
$d_3$	30.0	20.0	18.0	19.0

**Table B2.2** – IWRAP HH polarization  $d_0, d_1, d_2$  and  $d_3$  coefficients

Incidence	31°	36°	42°	49°
$d_0$	1.337E-1	-2.461E-1	2.864E-1	1.534E-1
$d_1$	8.883E-3	8.731E-2	-1.006E-3	3.223E-2
$d_2$	-1.121E-2	-8.289E-2	-3.737E-3	-3.438E-2
$d_3$	30.0	20.0	18.0	19.0